scientific reports

Check for updates

OPEN

A two phase differential evolution algorithm with perturbation and covariance matrix for PEMFC parameter estimation challenges

Mohammad Aljaidi[1]✉, Pradeep Jangir[2,3,4,5], Arpita[6], Sunilkumar P. Agrawal[7], Sundaram B. Pandya[8], Anil Parmar[8], G. Gulothungan[9]✉, Ali Fayez Alkoradees[10]✉ & Mohammad Khishe[11,12]✉

Parameter identification of Proton Exchange Membrane Fuel Cells (PEMFCs) is a key factor in improving the performance of the fuel cell and assuring the operational reliability. In this study, a novel algorithm PCM-DE, based on the Differential Evolution framework, is proposed. A perturbation mechanism along with a stagnation indicator based on a Covariance Matrix is incorporated into this algorithm. Three key innovations are introduced in the PCM-DE algorithm. A two phase approach based on fitness values is used to develop a parameter adaptation strategy, firstly. The idea here is to move the evolutionary process to more promising areas of the search space on different occasions. Second, a perturbation mechanism is incorporated that targets the archived population. This mechanism utilizes a novel weight coefficient, which is determined based on the fitness values and positional attributes of archived individuals, to improve exploration efficiency. Lastly, a stagnation indicator leveraging covariance matrix analysis is employed to evaluate the diversity within the population. This indicator identifies stagnant individuals and applies perturbations to them, promoting exploration and preventing premature convergence. The effectiveness of PCM-DE is validated against nine state-of-the-art algorithms, including TDE, PSO-sono, CS-DE, jSO, EDO, LSHADE, HSES, E-QUATRE, and EA4eig, through the parameter estimation of six PEMFC stacks—BCS 500 W, Nedstack 600 W PS6, SR-12 W, Horizon H-12, Ballard Mark V, and STD 250 W. Across all test cases, PCM-DE consistently achieved the lowest minimum SSE values, including 0.025493 for BCS 500 W, 0.275211 for Nedstack 600 W PS6, 0.242284 for SR-12 W, 0.102915 for Horizon H-12, 0.148632 for Ballard Mark V, and 0.283774 for STD 250 W. PCM-DE also demonstrated rapid convergence, superior robustness with the lowest standard deviations (e.g., 3.54E−16 for Nedstack 600 W PS6), and the highest computational efficiency, with runtimes as low as 0.191303 s. These numerical results emphasize PCM-DE's ability to outperform existing algorithms in accuracy, convergence speed, and consistency, showcasing its potential for advancing PEMFC modeling and optimization. Future research will explore PCM-DE's applicability to dynamic operating conditions and its adaptability to other energy systems, paving the way for efficient and sustainable fuel cell technologies.

Keywords Proton exchange membrane fuel cell (PEMFC), Parameter identification, Differential evolution, Perturbation mechanism, Metaheuristic algorithms

[1]Department of Computer Science, Faculty of Information Technology, Zarqa University, Zarqa 13110, Jordan. [2]University Centre for Research and Development, Chandigarh University, Gharuan, Mohali 140413, India. [3]Department of CSE, Graphic Era Hill University, Dehradun 248002, India. [4]Centre for Research Impact & Outcome, Chitkara University Institute of Engineering and Technology, Chitkara University, Rajpura, Punjab 140401, India. [5]Applied Science Research Center, Applied Science Private University, Amman 11937, Jordan. [6]Department of Biosciences, Saveetha School of Engineering, Saveetha Institute of Medical and Technical Sciences, Chennai 602 105, India. [7]Department of Electrical Engineering, Government Engineering College, Gandhinagar, Gujarat 382028, India. [8]Department of Electrical Engineering, Shri K.J. Polytechnic, Bharuch 392 001, India. [9]Department of Electronics and Communication Engineering, SRM Institute of Science and Technology, SRM Nagar, Kattankulathur, Chengalpattu, Tamilnadu 603203, India. [10]Unit of Scientific Research, Applied College, Qassim University, Buraydah, Saudi Arabia. [11]Department of Electrical Engineering, Imam Khomeini Naval Science University of Nowshahr,

Nowshahr, Iran. [12]Jadara University Research Center, Jadara University, Irbid, Jordan. ✉email: mjaidi@zu.edu.jo; g.gulothungan@gmail.com; alifk@qu.edu.sa; m_khishe@alumni.iust.ac.ir

Increasing global demand for clean and efficient sources of energy has increased the impetus on renewable technologies to be developed. Of these, Proton Exchange Membrane Fuel Cells (PEMFCs) are particularly attractive because of their high energy conversion efficiency, low operational temperature, ultra low emissions, and noiseless operation. Among allalternatives to fossil fuels, PEMFCs areregarded asone of the most promising, meeting global sustainability goals and the transition towards cleaner energy systems. Despite the advantages that PEMFCs have over other fuel cell types, their performance optimization is challenged by the inherent nonlinearity with complex internal reactions along with the dependence on semi empirical parameters. The development of reliable mathematical models that predict system behaviour under different operational conditions requires accurate estimation of PEMFC parameters. The I–V characteristics of PEMFCs are strongly dependent on these parameters, which include activation, ohmic, and concentration losses. However, due to the high nonlinearity and strong coupling in the system, it is difficult to identify these parameters using traditional methods. This problem needs advanced optimization techniques to solve it efficiently in high dimensional complex search spaces.

Previous research

Much is already known in the body of literature related to PEMFC parameter estimation, with many approaches relying on optimization algorithms and modeling techniques. Converged Moth Search Algorithm (CMSA) was introduced by Sun et al.[1] to minimize total squared deviations between experimental and simulated voltages on BCS 500-W PS6 and NedStack PS6 fuel cells. In parallel, Hao et al. developed an adaptive chaotic grey wolf optimization algorithm to enhance parameter estimation of solid oxide fuel cells (SOFCs). Applying their approach to a 5 kW dynamic tubular stack demonstrated improved convergence speed and accuracy over traditional methods[2]. The issue of gas starvation in PEMFCs was tackled by Yu et al.[3] using the Adaptive Network Based Fuzzy Inference System (ANFIS) to achieve 92% prediction accuracy and to provide a robust diagnostic framework. Du et al.[4] extended the application of ANFIS for fault diagnosis of offshore power systems using SCADA system data for precise short circuit fault identification.

Xing et al.[5] proposed a two stage adaptive parameter estimation framework for PEMFCs in the nonlinear modeling area, which was validated by experimental setups. A p dimensional extremum seeking optimization method that estimates unknown parameters in steady state PEMFC models was introduced by Yang et al.[6] and showed better accuracy and robustness than metaheuristic algorithms. The heterogeneous comprehensive learning Archimedes optimization algorithm (HCLAOA) was contributed by Fathy et al.[7] and tested on various PEMFC and SOFC stacks under different conditions and consistently yielded precise modeling. A review of a number of parameter estimation methods, such as artificial neural networks and bio inspired techniques, was carried out by Mitra et al.[8] with the view of optimizing fuel cell performance. Guo et al.[9] investigated particle swarm optimization to solve voltage imbalance in power distribution systems, but its direct applicability to PEMFC modeling is not clear.

For PEMFC parameter estimation, Yuan et al.[10] developed attack defense strategy assisted osprey optimization algorithm (ADSOOA), which shows better accuracy and convergence than existing methods on models such as BCS 500-W and NedStack PS6. The Black Widow Optimization (BWO) algorithm for PEMFC modeling was introduced by Singla et al.[11], which was found to perform better than the conventional optimization techniques. The field was advanced by Ghosh et al.[12] with their dynamic ant colony optimization (DACO) algorithm, which converged faster and more accurately to the parameter estimates. Singh et al.[13] suggested a hybrid algorithm by combining techniques of particle swarm optimization and dingo optimizer (DOX) to minimize errors in PEMFC models. A second hybrid approach, the Hybrid Particle Swarm Optimization Puffer Fish (HPSOPF) algorithm, also demonstrated robust parameter estimation for models such as Ballard Mark V and Avista SR 12[14].

Singla, et al.[15] also developed Enhanced Efficient Optimization Algorithm (EINFO), which provided faster convergence and lower squared errors in PEMFC parameter extraction. The Bi-Subgroup Optimization Algorithm (BSOA) was introduced by Chen et al.[16] which divides populations into exploratory and exploitative subgroups to improve diversity and accuracy of parameter estimation. The Bonobo Optimizer (BO) and its quasioppositional variant (QOBO) were used by Sultan et al.[17] and showed superior performance in PEMFC modeling compared to other optimization algorithms. For static PEMFC models, Mitra et al.[18] applied the Chaotic Embedded Particle Swarm Optimization (CEPSO) algorithm with high accuracy and efficiency.

Solid oxide fuel cells were focused on by Xiong et al.[19], who proposed the Simplified Competitive Swarm Optimizer (SCSO) to address the drawbacks of conventional swarm algorithms, but not applicable to PEMFCs. Thermal management in PEMFCs was reviewed by Yang et al.[20], and the importance of heat dissipation and control strategies for improved performance and reliability was stressed. In[21], Abdelmalek et al. optimized PEMFC based DC–DC converters using particle swarm optimization, resulting in superior voltage regulation and stability under varying conditions. A dynamic differential evolution algorithm (DDE-CGF) was proposed by Sun et al.[22] and showed faster convergence and higher accuracy in PEMFC parameter estimation.

A novel parameter identification method for dynamic PEMFC models with unmeasurable states is introduced by Li et al.[23], which yields higher accuracy and computational efficiency. Power electronic systems for fuel cell electric vehicles were reviewed by Rehman et al.[24] and challenges, trends, and future opportunities in this field were discussed. A temperature dependent piecewise modeling approach for PEMFCs was proposed by Bankupalli et al.[25] using fuzzy clustering and hybrid optimization to enhance accuracy at different operating conditions. To enhance real time operation and optimize PEMFC power output, Li et al.[26] used sliding mode variable structure control (SMVSC).

The Social Spider Algorithm (SSA) was improved by Kashefi et al.[27] for parameter estimation with high accuracy and convergence rates. The Weighted Mean of Vectors Optimizer was used by Lekouaghet et al.[28] for PEMFC parameter extraction, which outperformed other methods across many models. The Young's Double-Slit Experiment Optimizer (YDEO) was introduced by Tummala et al.[29] and shown to accurately identify parameters in benchmark PEMFC models. The Repairable Grey Wolf Optimization (RGWO) algorithm, which has improved exploration capabilities and robustness in parameter estimation, was presented by Ebrahimi et al.[30].

The LSHADE-EpSin optimization algorithm was used by Fathy et al.[31] for PEMFC modeling and shown to be effective on different commercial models. In[32], Alizadeh et al. combined a self consistent model with the SCCSA optimization algorithm, resolving inconsistencies in the literature and achieving high parameter estimation accuracy. Chen et al.[33] created a control oriented PEMFC system model based on fuzzy PID and RBF neural networks with significant improvement in temperature regulation. The hybrid cuckoo search—grey wolf optimization algorithm (CSGWO) was applied to SOFCs by Bai et al.[34], and they showed that it is efficient and robust. A hybrid fuzzy controller optimized by PSO was proposed by Wu et al.[35] to improve oxygen excess ratio control in PEMFC systems.

A hybrid grey wolf optimization method was introduced by Miao et al.[36] and the method was able to model PEMFC parameters efficiently with superior convergence[37]. An improved artificial bee colony algorithm (IABC) was applied for PEMFC models by Zhang et al.[38], which showed faster convergence and lower error rates. A novel particle swarm optimization initialization method for parameter estimation of nonlinear models was proposed by Ji et al.[39]. Mass transfer mechanisms in PEMFCs were reviewed by Yang et al.[40], who also discussed porous media dynamics[41] and parameter identification challenges. In[42], Sultan et al. assessed several metaheuristic optimization techniques, including Gazelle Optimization Algorithm (GOA), Prairie Dog Optimization (PDO), and Reptile Search Algorithm (RSA), and showed that they are effective for PEMFC modeling. In addition, Sultan et al.[43] proposed the modified manta ray foraging optimization (MMRFO) algorithm, which has the best performance in parameter estimation of different PEMFC stacks. A quasi dynamic model for a 3 kW PEMFC stack was developed by Yuan et al.[44] using hybrid genetic and PSO algorithms to predict voltage response accurately. Finally, the effect of temperature on PEMFC performance was investigated by Wei et al.[45], which shows dual effects on catalytic activity and thermal inconsistency induced degradation.

Research gap

Despite significant advancements in optimization techniques for parameter estimation in Proton Exchange Membrane Fuel Cells (PEMFCs), several gaps persist that hinder the development of more efficient and universally applicable algorithms. Existing methodologies, such as the Converged Moth Search Algorithm[1], adaptive chaotic grey wolf optimization[2], and hybrid metaheuristic approaches[13,14], have demonstrated improved accuracy, convergence speed, and robustness in specific scenarios. However, their applicability often remains limited to particular fuel cell models or operational conditions, reducing their generalizability across diverse PEMFC systems. Moreover, algorithms that have excelled on minimizing errors and allowing more precision such as LSHADE-EpSin[31] and Hybrid Particle Swarm Optimization-Puffer Fish (HPSOPF) algorithm[14] found pitfalls that, not only, deal with computational complexity, scalability with dynamic system, and vulnerability to local optima.

As the complexity of PEMFC systems increases and the parameter estimation problem becomes highly nonlinear and multivariable, algorithms are needed that can explore and exploit in a computationally efficient manner. In addition, current methods are not robust to real time dynamic conditions and unmeasurable states, which are essential for real world applications like fuel cell electric vehicles and power systems[23,24]. Moreover, most existing algorithms are designed to minimize a specific objective function, without considering the multi objective optimization scenarios where tradeoffs exist between accuracy, computational cost, and model robustness. These limitations point to a pressing need for new optimization algorithms that can address these issues, yielding higher accuracy, greater applicability and lower computational requirements for PEMFC parameter estimation.

PEMFCs display non-linear behavior because three main factors including electrochemical reaction mechanisms and material intrinsic properties unite with mass transport factors. The natural non-linear behavior exists in the electrochemical reactions that take place at both anode and cathode regions. The anode splits hydrogen molecules into protons and electrons but the cathode uses oxygen molecules with protons and electrons to create water. Overpotential and current density show a non-linear relationship according to the Butler-Volmer equation during these electrochemical reactions. The non-linearity of the system becomes more pronounced due to activation overpotential that depends on current density together with temperature and reactant concentration.

Mass transport limitations serve as a major non-linear factor that controls the movement of hydrogen and oxygen reactants and water removal from the system. Reaction sites within the porous electrodes and membrane experience decreased reactant concentration because of their diffusion from the gas channels which produces concentration overpotentials. The relationship between voltage and current density shows non-linearity because this process depends heavily on current density together with pressure and temperature conditions. The resistance to proton movement through the membrane together with electron flow through electrodes and external circuit generates additional non-linear effects known as ohmic losses. The membrane resistance shows strong dependence on its hydration state because current density and temperature fluctuations lead to an unstable ohmic overpotential. PEMFC performance depends heavily on temperature because it controls the reaction speed and proton mobility and gas diffusion processes. The non-linear correlations between temperature and these variables produce complex system behavior because their individual effects interact with one another. The operation of PEMFCs heavily depends on proper water management because membrane conductivity

requires an optimal water balance. The electrodes become flooded when water levels are too high which blocks gas diffusion yet insufficient water will cause membrane drying that decreases proton conductivity. The process of water content regulation depends on various factors including current density and temperature and reactant flow rates which results in highly non-linear behavior.

The PEMFC operations follow a non-linear path because numerous variables including electrochemical reactions, mass transfer resistances, electrical resistance and thermal conditions along with water control requirements. Exact models and complete knowledge of these influencing elements are essential to achieve optimized PEMFC operational performance while ensuring operational reliability.

This study becomes essential because traditional mathematical models fail to predict PEMFC parameters accurately. PEMFC modeling through conventional methods encounters difficulties in mimicking the nonlinear and interacting system behavior of such fuel cells during operational changes and theoretical or semi-empirical analytical methods prove insufficient in this regard. PEMFC modeling accuracy together with predictive reliability in practical applications depends directly on the precise estimation of activation overpotential and ohmic resistance and concentration losses. The current mathematical models incorporate pre-defined simplifications with assumptions which cause observed differences between their predictions and actual field conditions. The models lack capability to incorporate dynamic temperature changes alongside humidity fluctuations and reactant pressure variations because these factors substantially impact PEMFC operation. The calculation of electrochemical and transport parameters becomes difficult because optimization landscape features numerous local minima that standard gradient-based approaches cannot efficiently optimize and tend to result in suboptimal solutions.

Advanced optimization approaches need to be implemented for PEMFC model parameter estimation because they solve current challenges. The Perturbation and Covariance Matrix-based Differential Evolution (PCM-DE) algorithm incorporates three fundamental components that include a two-stage parameter adjustment system and a perturbation method for better exploration as well as a covariance matrix-based stagnation detection system for population diversity preservation. The optimization procedure makes dynamic parameter value adjustments and exploits the search space efficiently while preventing premature convergence because of these three implemented mechanisms which ultimately delivers advanced accuracy and robustness compared to contemporary state-of-the-art algorithms. The research connects theoretical PEMFC modeling with practical optimization through an efficient method to determine model parameters. The superior accuracy together with reliable stability and fast convergence makes metaheuristic algorithms essential above mathematical models for finders. The research results enhance PEMFC model predictive reliability which enables their use in energy systems and fuel cell electric vehicles and hybrid renewable applications.

This paper introduces a novel optimization approach based on Differential Evolution, enhanced with Perturbation Mechanism and Covariance Matrix-based stagnation indicators (PCM-DE)[46], for the parameter identification of PEMFCs. The primary contributions are as follows:

- *Two-phase Parameter Adaptation*: A fitness-value-based adaptation strategy that dynamically balances exploration and exploitation across evolutionary stages.
- *Perturbation Mechanism*: A novel weight coefficient leveraging fitness and position information to guide the search process effectively.
- *Covariance Matrix-based Stagnation Indicator*: A statistical measure of population diversity, used to perturb stagnant individuals and maintain exploration capabilities.
- *Performance Validation*: The proposed PCM-DE algorithm is applied to six PEMFC stacks (BCS 500 W[17,47], Nedstack 600 W PS6[17,47], SR-12 W[17,47], Horizon H-12[48], Ballard Mark V[48], and STD 250 W[49]) and benchmarked against nine state-of-the-art optimization techniques, including Two-stage Differential Evolution (TDE)[50], PSO-sono[51], Cooperative strategy based differential evolution (CS-DE)[52], jSO[53], Exponential Distribution Optimizer (EDO)[54], LSHADE[55], Hybrid Sampling Evolutionary Strategy (HSES)[56], E-QUATRE[57], and EA4eig[58].
- *Comprehensive Evaluation*: The study evaluates PCM-DE using Sum of Squares Error (SSE) and statistical measures to demonstrate its robustness, accuracy, and convergence efficiency.

The PCM-DE algorithm addresses critical limitations of existing approaches by incorporating novel mechanisms for adaptive parameter tuning and diversity maintenance. Its ability to achieve superior performance across multiple PEMFC models highlights its potential as a scalable and robust optimization tool. Furthermore, the proposed method enhances the understanding of optimization strategies in nonlinear systems, contributing to the broader field of renewable energy research.

The remainder of the paper is structured as follows: Section "PEMFC mathematical modelling" explains the Mathematical modeling of PEMFCs, detailing the equations governing their I–V characteristics. Section "PCM-DE algorithm : evolution and mathematical modelling" introduces the PCM-DE algorithm, including its theoretical framework and implementation details. Results and discussion, presenting comparative analysis, statistical validation, and insights from the optimization outcomes are explained in Section "Result analysis for PEMFC parameter optimization". Finally, Section "Conclusion" ends with Conclusions and future work, summarizing findings and proposing directions for further research.

PEMFC mathematical modelling

Basic concept of PEMFC

The Proton Exchange Membrane Fuel Cell (PEMFC) structure includes two electrodes, specifically the anode and the cathode, and a proton-conducting membrane positioned between these electrodes as the polymer electrolyte. The schematic diagram of fuel cell is given in Fig. 1.

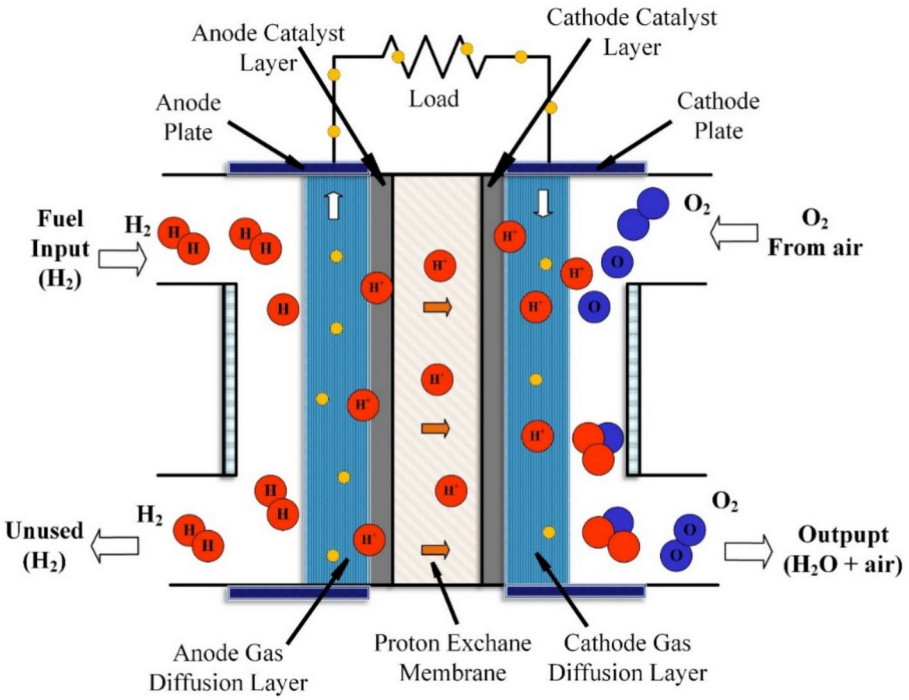

Fig. 1. Schematic of fuell cell.

This configuration allows protons to pass through while preventing the flow of electrons, as described in[59]. Catalyst layers are positioned between the electrolyte membrane and the electrodes to accelerate the chemical reactions. At the anode electrode, hydrogen gas is introduced and dissociates into electrons and protons upon reaching the catalytic layer. The protons traverse the electrolyte membrane to the catalytic layer at the cathode electrode, while the electrons flow through an external load. Oxygen or air is supplied to the cathode electrode, where it interacts at the catalytic layer with protons transported from the membrane and electrons arriving from the external circuit, resulting in the formation of water. The electrochemical reactions occurring at the electrodes of the PEMFC are represented as follows:

Anode reaction

$$\mathrm{H_2} \rightarrow 2\mathrm{H^+} + 2\mathrm{e^-} \tag{1}$$

Cathode reaction

$$2\mathrm{H^+} + \tfrac{1}{2}\mathrm{O_2} \rightarrow \mathrm{H_2O} \tag{2}$$

Overall reaction:

$$\mathrm{H_2} + \tfrac{1}{2}\mathrm{O_2} \rightarrow \mathrm{H_2O} + \mathrm{Energy} + \mathrm{Heat} \tag{3}$$

In Eq. (3), the term "Energy" represents the electrical energy generated as a result of electron flow from hydrogen gas traveling from the anode to the cathode through an external load. The equivalent electrical circuit for PEMFC stack is shown in Fig. 2.

Mathematical model of PEMFC stacks

The output voltage V_{cell} of each individual fuel cell can be computed using the following expression[60,61]:

$$V_{\mathrm{cell}} = E_{\mathrm{nerst}} - \Delta V_{\mathrm{act}} - \Delta V_{\mathrm{ohm}} - \Delta V_{\mathrm{con}} \tag{4}$$

In this equation, E_{nerst} denotes the open-circuit voltage of the cell, ΔV_{act} represents the activation overpotential per cell, ΔV_{ohm} describes the voltage drop caused by ohmic resistance due to electron conduction through the external load and the proton movement resistance in the electrolyte membrane, and ΔV_{con} indicates the concentration overpotential per cell. Amphlett et al.[62] proposed a model of a fuel cell's electrochemical properties. When a series connection of N_{cells} identical fuel cells is configured for increased voltage output, the total stack voltage can be determined as:

$$V_{\mathrm{stack}} = N_{\mathrm{cells}} \cdot V_{\mathrm{cell}} \tag{5}$$

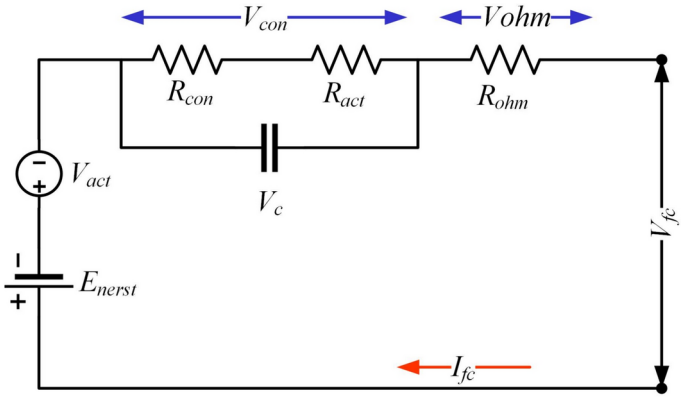

Fig. 2. Equivalent electrical circuit for PEMFC.

Here, N_{cells} refers to the number of cells connected in series, and V_{cell} is the output voltage for each individual fuel cell, as derived from Eq. (4).

The reversible potential, E_{nerst}, is calculated as follows[63,64]:

$$E_{nerst} = 1.229 - 8.5 \times 10^{-4} \left(T_{\text{fc}} - 298.15\right) + 4.3085 \times 10^{-5} T_{\text{fc}} \cdot \left[\ln\left(P_{\text{H}_2}\right) + \ln\left(\sqrt{P_{\text{O}_2}}\right)\right] \tag{6}$$

where T_{fc} is the cell's absolute operating temperature in Kelvin, while P_{H_2} and P_{O_2} denote the partial pressures of hydrogen and oxygen in the fuel cell stack's input channels (atm). When hydrogen and air serve as the inputs, the partial oxygen pressure, P_{O_2}, is determined as follows[65,66]:

$$P_{\text{O}_2} = P_{\text{c}} - RH_{\text{c}} P^{\text{sat}}_{\text{H}_2\text{O}} - \frac{0.79}{0.21} P_{\text{O}_2} \cdot \exp\left(0.291 \frac{I_{\text{fc}}}{A} / T^{0.832}_{\text{fc}}\right) \tag{7}$$

where P_{c} represents the inlet channel pressure at the cathode (atm), RH_{c} is the cathode electrode's relative humidity, I_{fc} is the operating current (A), A is the membrane surface area (cm^2), and $P^{\text{sat}}_{\text{H}_2\text{O}}$ is the water vapor pressure at saturation, defined by[67]:

$$\begin{aligned} \log_{10}\left(P^{\text{sat}}_{\text{H}_2\text{O}}\right) = {} & 2.95 \times 10^{-2} \left(T_{\text{fc}} - 273.15\right) - 9.18 \times 10^{-5} \left(T_{\text{fc}} - 273.15\right)^2 \\ & + 1.44 \times 10^{-7} \left(T_{\text{fc}} - 273.15\right)^3 - 2.18 \end{aligned} \tag{8}$$

In cases where hydrogen and pure oxygen are used, the partial oxygen pressure P_{O_2} is calculated as follows:

$$P_{\text{O}_2} = RH_{\text{c}} P^{\text{sat}}_{\text{H}_2\text{O}} \left[\left(\exp\left(4.192 \frac{1}{I_{\text{fc}}} / T^{1.334}_{\text{fc}}\right) \cdot \frac{RH_{\text{c}} P^{\text{sat}}_{\text{H}_2\text{O}}}{P_{\text{a}}}\right)^{-1} - 1\right] \tag{9}$$

In both cases, the partial hydrogen pressure P_{H_2} is given by:

$$P_{\text{H}_2} = 0.5 RH_{\text{a}} P^{\text{sat}}_{\text{H}_2\text{O}} \left[\left(\exp\left(1.635 \frac{1}{I_{\text{fc}}} / T^{1.334}_{\text{fc}}\right) \cdot \frac{RH_{\text{a}} P^{\text{sat}}_{\text{H}_2\text{O}}}{P_{\text{a}}}\right)^{-1} - 1\right] \tag{10}$$

where P_{a} is the anode electrode's inlet channel pressure (atm), and RH_{a} indicates the relative humidity on the anode side.

The activation voltage drop ΔV_{act} for the electrodes is calculated by:

$$\Delta V_{\text{act}} = -\left[\xi_1 + \xi_2 T_{\text{fc}} + \xi_3 T_{\text{fc}} \ln\left(C_{\text{O}_2}\right) + \xi_4 T_{\text{fc}} \ln\left(I_{\text{fc}}\right)\right] \tag{11}$$

where ξ_1, ξ_2, ξ_3, and ξ_4 are empirical coefficients, and C_{O_2} denotes the oxygen concentration at the cathode (mol/cm^3) The activation overpotential, represented by Eq. (11), is derived from the electrochemical kinetics of the fuel cell reactions and is influenced by several factors, including the reaction mechanism, catalyst type, and operating conditions. The activation overpotential depends on the electrochemical reactions at the anode and cathode involve the transfer of electrons and protons. The activation overpotential is influenced by the rate of these reactions, which is governed by the Arrhenius equation and the Butler-Volmer equation. The empirical coefficients ξ_1, ξ_2, ξ_3, and ξ_4 capture the dependence of the reaction rate on temperature, reactant concentration, and current density.

The type of catalyst used in the fuel cell significantly affects the activation overpotential. For example, platinum (Pt) is commonly used as a catalyst in Proton Exchange Membrane Fuel Cells (PEMFCs) due to its high activity for hydrogen oxidation and oxygen reduction reactions. The catalyst's surface area, morphology, and

loading influence the activation overpotential. The activation overpotential is temperature-dependent, as higher temperatures generally enhance reaction kinetics, reducing the overpotential. This dependence is captured by the terms involving T_{fc} in Eq. (11). The concentration of oxygen at the cathode affects the reaction rate and, consequently, the activation overpotential. Lower oxygen concentrations increase the overpotential due to reduced reactant availability, as reflected in the term $\xi_3 T_{\mathrm{fc}} \ln\left(C_{\mathrm{O}_2}\right)$. The activation overpotential increases with current density, as higher currents require more energy to drive the electrochemical reactions. This relationship is represented by the term $\xi_4 T_{\mathrm{fc}} \ln\left(I_{\mathrm{fc}}\right)$. Equation (11) is obtained by modeling the activation overpotential as a function of temperature, oxygen concentration, and current density, with empirical coefficients that account for the specific characteristics of the fuel cell, such as the catalyst type and reaction kinetics. This equation is widely used in PEMFC modeling to accurately capture the voltage losses associated with activation overpotential as follows:

$$C_{\mathrm{O}_2} = \frac{P_{\mathrm{O}_2}}{5.08\times10^6 \cdot \exp(-498/f_{\mathrm{fc}})} \tag{12}$$

The ohmic resistive voltage drop ΔV_{ohm} is determined by:

$$\Delta V_{\mathrm{ohm}} = I_{\mathrm{fc}}\left(R_M + R_C\right) \tag{13}$$

where R_M is the membrane resistance (Ω) and R_C is the resistance due to proton movement through the membrane. The main difference between membrane resistance (R_M) and the resistance due to proton movement through the membrane (R_C) lies in their physical origins and contributions to the overall voltage loss in a Proton Exchange Membrane Fuel Cell (PEMFC). Membrane resistance (R_M) arises from the intrinsic electrical resistivity of the polymer electrolyte membrane itself, which governs the ease with which protons can traverse the membrane from the anode to the cathode. This resistance is influenced by factors such as membrane thickness, hydration level, and ionic conductivity. A well-hydrated membrane exhibits lower resistance due to enhanced proton conduction through the hydrated ionic pathways. On the other hand, the resistance due to proton movement through the membrane (R_C) accounts for additional resistive losses encountered by protons as they migrate through the electrolyte. This resistance incorporates the effects of water content, local temperature variations, and the structural properties of the membrane, such as its degree of swelling or compression under operating conditions. Unlike R_M, which primarily depends on the material properties of the membrane, R_C also reflects dynamic operational influences that impact proton transport efficiency. R_M represents the inherent resistivity of the membrane material, while R_C encompasses the additional resistance associated with the actual proton migration process under real operating conditions. Both resistances collectively contribute to the ohmic losses in the PEMFC, affecting its overall efficiency and performance.

Membrane resistance is calculated as:

$$R_M = \frac{\rho_M \cdot l}{A} \tag{14}$$

with ρ_M being specific membrane resistance (Ω·cm), representing membrane thickness (cm), and the empirical formula for ρ_M given as:

$$\rho_M = \frac{181.6\left[1 + 0.03\left(\frac{I_{fc}}{A}\right) + 0.062\left(\frac{T_{fc}}{303}\right)^2\left(\frac{I_{fc}}{A}\right)^{2.5}\right]}{\left[\lambda - 0.634 - 3\left(\frac{I_{fc}}{A}\right)\right] \times \exp\left[4.18\left(\frac{T_{fc}-303}{T_{fc}}\right)\right]} \tag{15}$$

where λ is an adjustable parameter connected to membrane preparation.

The concentration voltage drop, ΔV_{con}, is determined by:

$$\Delta V_{con} = -b \ln\left(1 - \frac{J}{J_{\max}}\right) \tag{16}$$

In this context, b represents a parametric coefficient (V), while J and $J_{\max}$ denote the current density and the maximum current density (A/cm^2), respectively. For accurate modeling under simulation and control conditions, precise estimation of these parameters is critical. The optimization process involves determining seven unknown parameters ($\xi_1, \xi_2, \xi_3, \xi_4, \lambda, R_C$, and b) using the CHHO optimization technique.

Objective function

To closely align the model output with experimental PEMFC data, the optimization problem is solved by employing the SAO-MPSO technique, minimizing the sum of squared errors (SSE) between experimentally measured and calculated stack voltages[68,69]:

$$OF = \min SSE\left(x\right) = \min \sum_{i=1}^{N}\left[v_{\mathrm{meas}}\left(i\right) - v_{\mathrm{cal}}\left(i\right)\right]^2 \tag{17}$$

where x represents the unknown parameter vector, N is the number of data points, i is the iteration index, v_{meas} is the measured PEMFC voltage, and v_{cal} is the estimated voltage. The optimization is subject to the following constraints:

$$\begin{aligned} \xi_{i,\min} \leq \xi_i \leq \xi_{i,\max},\ i = 1:4 \\ R_{C\min} \leq R_C \leq R_{C\max} \\ \lambda_{\min} \leq \lambda \leq \lambda_{\max} \\ b_{\min} \leq b \leq b_{\max} \end{aligned} \tag{18}$$

where $\xi_{i,\min}$ and $\xi_{i,\max}$ are the limits for empirical coefficients, $R_{C,\min}$ and $R_{C,\max}$ are resistance bounds, and $\lambda_{\min}$, $\lambda_{\max}$, $b_{\min}$, and $b_{\max}$ define the limits for water content and parametric coefficients. The mean bias error for voltage is calculated as per below equation:

$$MBE = \frac{\sum_{i=1}^{N} |V_{meas}(i) - V_{calc}(i)|}{N} \tag{19}$$

PCM-DE algorithm : evolution and mathematical modelling

This section discusses the foundational operations of the Differential Evolution (DE) algorithm and sequentially explains the modifications implemented to develop the PCM-DE algorithm.

Basic operations of differential evolution

The Differential Evolution (DE) algorithm operates in two primary stages: initialization and evolution. During initialization, a random population is generated, while in the evolution stage, the population undergoes three core operations—mutation, crossover, and selection. These steps are repeated until the termination criteria are satisfied.

Initialization

The initialization process is the first step toward exploring the global optimal solution in a D-dimensional search space. For practical purposes, each dimension of the candidate solutions is bounded within specific limits. The target vector is expressed as:

$$X_{i,G} = [X_{i,1,G}, X_{i,2,G}, \ldots, X_{i,D,G}],\ i = 1, 2, \ldots, PS \tag{20}$$

Here, $X_{i,G}$ represents the i-th candidate solution in the G-th generation, and D indicates the dimensionality of the individual. Each dimension of the i-th individual is generated using:

$$X_{i,j} = X_{\min,j} + \text{rand}(0,1) \cdot (X_{\max,j} - X_{\min,j}) \tag{21}$$

In this equation, $X_{\max,j}$ and $X_{\min,j}$ denote the upper and lower bounds for the j-th dimension, respectively, and $\text{rand}(0,1)$ is a uniformly distributed random number within the range $[0,1]$.

Mutation

In the mutation process, a mutant vector $V_{i,G}$ is generated by combining the target vector with a difference vector. Different mutation strategies are used depending on the optimization problem, as described below:

- DE/rand/1:

$$V_{i,G} = X_{r_0,G} + F \cdot (X_{r_1,G} - X_{r_2,G}) \tag{22}$$

- DE/best/1:

$$V_{i,G} = X_{\text{best},G} + F \cdot (X_{r_1,G} - X_{r_2,G}) \tag{23}$$

- DE/rand/2:

$$V_{i,G} = X_{r_0,G} + F \cdot (X_{r_1,G} - X_{r_2,G}) + F \cdot (X_{r_3,G} - X_{r_4,G}) \tag{24}$$

- DE/best/2:

$$V_{i,G} = X_{\text{best},G} + F \cdot (X_{r_1,G} - X_{r_2,G}) + F \cdot (X_{r_3,G} - X_{r_4,G}) \tag{25}$$

- DE/target-to-best/1:

$$V_{i,G} = X_{i,G} + F \cdot (X_{\text{best},G} - X_{i,G}) + F \cdot (X_{r_1,G} - X_{r_2,G}) \tag{26}$$

- DE/rand/2/dir:

$$V_{i,G} = X_{r_1,G} + \tfrac{F}{2} \cdot (X_{r_1,G} - X_{r_2,G} - X_{r_3,G}) \tag{27}$$

In these equations, r_0, r_1, r_2, r_3, and r_4 are unique integers selected randomly from the set $\{1, 2, \ldots, PS\}$. The term $X_{\text{best},G}$ represents the best vector in the G-th generation, and F is the scaling factor that determines the magnitude of the difference vector.

Crossover
The crossover operation generates a trial vector $U_{i,G}$ by combining the mutant vector $V_{i,G}$ with the target vector $X_{i,G}$. The process is defined as:

$$U_{j,i,G} = \begin{cases} V_{j,i,G}, & \text{if rand}\,(0,1) \le CR_i \text{ or } j = j_{\text{rand}} \\ X_{j,i,G}, & \text{otherwise} \end{cases} \tag{28}$$

Here, j_{rand} is a randomly chosen integer within the range $[1, D]$, ensuring that at least one dimension of the donor vector is inherited. The crossover rate (CR) governs the number of dimensions taken from the mutant vector.

Selection
Selection determines whether the trial vector or its corresponding target vector advances to the next generation. The fitness of all trial vectors is evaluated, and the vector with the better fitness value is retained. The selection process is expressed as:

$$X_{i,G+1} = \begin{cases} U_{i,G}, & \text{if } f\left(U_{i,G}\right) < f\left(X_{i,G}\right) \\ X_{i,G}, & \text{otherwise} \end{cases} \tag{29}$$

The proposed PCM-DE algorithm

The PCM-DE algorithm incorporates three main innovations: a two-phase parameter adaptation strategy, a perturbation mechanism for the archived population, and a population diversity enhancement mechanism based on a covariance matrix.

Two-phase parameter adaptation strategy
In DE, sensitivity to control parameters often limits optimization performance. The parameter F, which scales the difference vector, is particularly critical. In PCM-DE, F is adapted using a two-phase strategy. During the initial phase, F is generated using a wavelet basis function to capture both gradual and rapid variations, maintaining values within the range [0.4,0.6]. This approach minimizes premature convergence. In the latter phase, F follows a Cauchy distribution, $F \sim C(\mu_F, 0.1)$, ensuring adequate exploration.

The crossover rate (CR) is also dynamically adjusted. In the early stages of evolution, higher CR values are used to promote global exploration, while lower values facilitate exploitation in later stages. CR follows a Gaussian distribution, $CR \sim C(\mu_{CR}, 0.1)$.

Historical memory values are updated for successful parameter adjustments to enhance adaptability throughout the optimization process.

The generation of F and CR is described by the following equations:

$$F_i = \begin{cases} \sqrt{2}\pi^{-1/3} \cdot \left(1 - \mu_{F,r_i}^2\right) \cdot e^{-\mu_{F,r_i}^2 + 0.1 \cdot \text{rand}_i}, & \text{if nfes} < \perp \\ \text{randc}_i\left(\mu_{F,r_i}, 0.1\right), & \text{otherwise} \end{cases} \tag{30}$$

$$CR_i = \begin{cases} 0, & \text{if } \mu_{CR,r_i} = \emptyset \\ \text{randn}_i\left(\mu_{CR,r_i}, 0.1\right), & \text{otherwise} \end{cases} \tag{31}$$

$$CR_i = \begin{cases} \max\left(CR_i, 0.6\right), & \text{if nfes} < \perp \\ \max\left(CR_i, 0\right),\ \min\left(CR_i, 1\right), & \text{otherwise} \end{cases} \tag{32}$$

In these equations, μ_{F,r_i} and μ_{CR,r_i} denote control parameters selected randomly from the H entries of the memory pool, and $\perp$ represents the threshold between the two evolutionary phases, set at $\text{nfes}_{\max} \cdot 0.2$. randn_i and randc_i correspond to Gaussian and Cauchy distributions, respectively.

Historical memory values μ_F and μ_{CR} are updated at the end of each generation. When a trial vector outperforms its target vector, CR_i and F_i are stored as S_{CR} and S_F, respectively, in the successful parameter set. The adaptation equations are as follows:

$$w_k = \frac{\Delta f_k}{\sum_{k=1}^{|S_F|} \Delta f_k},\ \Delta f_k = \left|f\left(X_{i,G}\right) - f\left(U_{i,G}\right)\right|$$

$$\text{mean}_{WL}\left(S_F\right) = \frac{\sum_{k=1}^{|S_F|} w_k \cdot S_F^2\left(k\right)}{\sum_{k=1}^{|S_F|} w_k \cdot S_F\left(k\right)}$$

$$\mu_{F,k,G+1} = \begin{cases} \text{mean}_{WL}\left(S_F\right), & \text{if } S_F \neq 0 \\ \mu_{F,k,G}, & \text{otherwise} \end{cases} \tag{33}$$

Similarly:

$$\text{mean}_{WL}\left(S_{CR}\right)=\frac{\sum_{k=1}^{|S_{CR}|} w_k \cdot S_{CR}^2(k)}{\sum_{k=1}^{|S_{CR}|} w_k \cdot S_{CR}(k)}$$

$$\mu_{CR,k,G+1}=\begin{cases}\text{mean}_{WL}\left(S_{CR}\right), & \text{if } S_{CR}\neq 0\\ \mu_{CR,k,G}, & \text{otherwise}\end{cases} \tag{34}$$

Additionally, population size (PS) is reduced as follows:

$$PS_{G+1}=\text{round}\left[\frac{PS_{\min}-PS_{\max}}{\text{nfes}_{\max}}\cdot \text{nfes}+PS_{\max}\right] \tag{35}$$

Here, $PS_{\min}$ and $PS_{\max}$ represent the minimum and maximum population sizes, respectively.

Perturbation mechanism for archived population

The mutation strategy significantly influences the search direction in Differential Evolution (DE). To achieve a balance between exploration and exploitation, the DE/target-to-pbest/1 strategy, as introduced in[70], is applied in the PCM-DE algorithm. This strategy utilizes an external archive that retains the inferior individuals discarded during the selection process, thereby improving population diversity. The mutant vector is defined as:

$$V_{i,G}=X_{i,G}+F\cdot\left(X_{\text{best},G}^{p}-X_{i,G}\right)+F\cdot\left(X_{r_1,G}-\tilde{X}_{r_2,G}\right) \tag{36}$$

In this equation:

- $X_{\text{best},G}^{p}$ is randomly chosen from the top 100 p% of individuals, where $p\in(0,1]$.
- X_i and X_{r_1} are selected from P, the current population.
- $\tilde{X}_{r_2}$ is selected from the combined set of P (current population) and A (external archive).

Although the use of inferior individuals contributes to diversity, their effectiveness can decline if they remain unmodified during evolution. Additionally, the "one-to-one" competition mechanism in DE ensures that trial vectors only compete against their respective target vectors. Even if a target vector loses in competition, it might still have better fitness than other population members.

To address these challenges, a perturbation mechanism based on an exponential distribution is introduced to renew archived individuals, ensuring better utilization. A quarter of the archived individuals are randomly chosen for perturbation. This reduces potential bias and resolves issues arising from suboptimal parameter assignments, such as scaling factor F, crossover rate CR, or both. The perturbation mechanism is formulated as: $LF_i=\frac{f(X_{i,G})}{f(U_{i,G})+f(X_{\text{best},G})}$, $ELF=k\cdot e^{k\cdot LF}$

The updated archive individual is given by:

$$\tilde{X}_{r_2}=\tilde{X}_{r_2}+ELF\cdot\left(X_{\text{best}}^{p}-\tilde{X}_{r_2}\right) \tag{37}$$

Population diversity enhancement mechanism based on covariance matrix

Population diversity evolves dynamically throughout the optimization process. High diversity is critical during the initial exploration phase to identify promising regions of the search space, while reduced diversity facilitates exploitation in the later stages to refine solutions. However, excessive loss of diversity may result in stagnation or premature convergence.

To monitor and maintain diversity, a covariance matrix is constructed to analyze the spatial distribution of individuals. This matrix tracks the spread of individuals within the search space. A counter (Co) records the number of individuals whose variance falls below a threshold of 0.00001. When the counter surpasses a predefined threshold (N_1), stagnation is assumed, and the stagnant individuals undergo perturbation. The perturbation process is described using the equation:

$$CQ_G=Q_G\cdot\sum_{k=1}^{PS}\left(\left(X_{i,k,G}-\overline{X}_{i,G}\right)\cdot\left(X_{j,k,G}-\overline{X}_{j,G}\right)\right) \tag{38}$$

In this equation:

- Q_G represents the eigenvector matrix of the covariance matrix.
- Q_G^{-1} denotes the inverse of the eigenvector matrix.

This mechanism ensures that diversity is preserved throughout the evolutionary process, preventing stagnation and enhancing the algorithm's ability to explore and exploit effectively.

```
for i = 1 to PS do
    if f(X_{i,G}) > f(U_{i,G}) then
        count(i) = count(i) + 1
    else
        count(i) = 0;
    end if
end for
```

Algorithm 1. Calculate *count*

During the evolutionary process, certain individuals may become trapped in local optima, leading to stagnation. These individuals are identified as stagnant individuals. A counter is used to track their total number. When predefined conditions are met, the stagnation mechanism is triggered. The threshold for this mechanism is represented by N_2, defined as $2 - D$. Once the threshold is reached, stagnant individuals are updated using the following equation:

$$X_{i,G} = CQ_{i,G} + X_{i,G} \tag{39}$$

In this equation, $X_{i,G}$ represents the stagnant individual, while $CQ_{i,G}$ signifies the normalization of individuals within the population using the covariance matrix.

Input: Maximum number of function evaluations $nfes_{\max}$, objective function $f(X)$, constraint boundary $[UB, LB]$
Output: Global optimal solution X_{best} and its fitness $f(X_{\text{best}})$;

for $i = 1$ to PS **do**
  $X_{i,G} = X_i$; Calculate $f(X_{i,G})$;
end for
Find the global best $X_{\text{gbest},G}$ and fitness value $f(X_{\text{gbest},G})$;
while $nfes < nfes_{\max}$ **do**
  $S_{CR} = \emptyset, S_F = \emptyset$;
  for $i = 1$ to PS **do**;
    $r_i =$ Select from $[1, H]$ randomly;
    if $\mu_{CR,r_i} = \perp, CR_{i,G} = 0$. Otherwise **then**
    end if
    Assign F and CR to each individual using; (Eqs. (30) and (31) and (32));
  end for
  for $i = 1$ to PS **do**
    if $f(U_{i,G} \leq f(X_{i,G})$ **then**
      $X_{i,G+1} = U_{i,G}$;
    else
      $X_{i,G+1} = X_{i,G}$;
    end if
    if $f(U_i < f(X_{i,G}))$ **then**
      $X_{i,G} \rightarrow A$;
      $CR_{i,G} \rightarrow S_{CR}, F_{i,G} \rightarrow S_F$;
    end if
  end for
  Update μ_{CR} and μ_F according to Eqs. (33) and (34);
  Calculate A according to Eq. (37);
  It will be randomly removed from the archive, making the population size save A;
  Execute Algorithm 1;
  for $j = 1$ to D **do**
    if $Co(j,j) > N_1$ **then**
      for $i = 1$ to PS **do**
        if $count(i) > N_2$ **then**
          Calculate $X_{i,G}$ according to Eq. (39);
          Calculate the fitness value $f(X_{i,G})$;
          $nfes = nfes + 1$;
          $count(i) = 0$;;
          end if
      end for
    $Co(j,j) = 0$;;
  end if
  end for
  Calculate PS_{G+1} according to Eq. (35);
  $G = G + 1$;;
end while

Algorithm 2. Pseudocode of PCM-DE

Result analysis for PEMFC parameter optimization

Result analysis

This study is structured in the computational framework to assess the performance of the proposed Perturbation and Covariance Matrix based Differential Evolution (PCM-DE) algorithm in the optimization of the parameters of six Proton Exchange Membrane Fuel Cell (PEMFC) stacks. The system used for implementation was an Intel Core i5-10400F processor at 2.90 GHz, 16 GB RAM and Windows 7 (64-bit) operating system. Algorithm development and testing were performed in MATLAB 2021b. For each optimization run, the PCM-DE algorithm

S. no	PEMFC type	Power (W)	Ncells (no)	A (cm^2)	L (um)	T (K)	J_{max} (mA/cm^2)	PH_2 (bar)	PO_2 (bar)
CASE 1	BCS 500 W	500	32	64	178	333	469	1.0	0.2095
CASE 2	NetStack PS6	6000	65	240	178	343	1125	1.0	1.0
CASE 3	SR-12	500	48	62.5	25	323	672	1.47628	0.2095
CASE 4	Horizon H-12	12	13	8.1	25	328.15	246.9	0.4935	1.0
CASE 5	Ballard Mark V	5000	35	232	178	343	1500	1.0	1.0
CASE 6	STD 250 W	250	24	27	127	343	860	1.0	1.0

Table 1. Case studies classification based on PEMFC characteristics.

Algorithm	Parameter setting
TDE (Two-stage Differential Evolution)	$\mu F = 0.3,\ \mu CR = 0.8,\ F\&CR\ same\ as\ LSHADE,\ p = 0.11,$ $PS = 25 \times \ln(D) \times \sqrt{D} \sim 4,\ rrac,$ $A = 1.6,\ rrac,\ B = 3,\ p = 2/3 \times nfes\max$
PSO-sono	$PS = 100,\ r = 0.5,\ \epsilon = D/PS \times 0.01,\ iw \in [0.4, 0.9]$
CS-DE (Cooperative strategy based differential evolution)	$\mu F = 0.8,\ \mu CR = 0.6,\ F\&CR\ same\ as\ LSHADE,\ p = 0.25 \sim 0.05,$ $PS = 25 \times \ln(D) \times \sqrt{D} \sim 4,\ rrac = 1.6,\ rrac,$ $A = 1.6,\ rrac,\ B = 5,\ T0 = G\max/2,\ K = 4$
jSO	$\mu F = 0.3,\ \mu CR = 0.8,\ F,\ CR\&\ rrac\ same\ as\ LSHADE,$ $PS = 25 \times \ln(D) \times \sqrt{D} \sim 4,\ p = 0.25 \sim 0.125,\ H = 5$
EDO (Exponential Distribution Optimizer)	$\alpha = 0.25$
LSHADE	$\mu F = 0.5,\ \mu CR = 0.5,\ F \sim C(\mu F,\ 0.1),$ $PS = 18 \times D \sim 4,\ CR \sim C(\mu CR,\ 0.1),\ rrac = 2.6,\ p = 0.11,\ H = 6$
HSES (Hybrid Sampling Evolutionary Strategy)	$cc = 0.96,\ I = 20,\ M = 200,\ PS = 100$
E-QUATRE	$PS = 100,\ T0 = 70,\ p\max = 0.2,\ p\min = 0,\ rrac = 1.6$
EA4eig	$PSini = 100,\ PSmin = 10,\ qh = 1/H,\ H = 4$
PCM-DE	$\mu F = 0.5,\ \mu CR = 0.8,\ F\&CR\ same\ as\ LSHADE,\ p = 0.11,\ rrac = 1.4,$ $PS = 25 \times \ln(D) \times \sqrt{D} \sim 4,\ H = 4,\ N2 = 2 \times D,\ N1 = 0.0001,\ k = 4 \sim 40$

Table 2. Parameter setting of different DE and Non-DE algorithms used.

was configured with a population size of 50 and a maximum of 500 iterations. Sum of Squares Error (SSE) was used as the fitness function, which is the difference between the measured and modeled voltage values of PEMFCs. The algorithm introduced three innovative mechanisms to address challenges in parameter identification: a two-phase parameter adaptation strategy for dynamic fitness-based exploration, a perturbation mechanism leveraging archived populations, and a covariance matrix-based stagnation indicator for maintaining diversity and avoiding premature convergence. To validate the robustness and efficiency of PCM-DE, its performance was benchmarked against nine state-of-the-art algorithms: TDE, PSO-sono, CS-DE, jSO, EDO, LSHADE[71], HSES, E-QUATRE, and EA4eig. These algorithms were chosen to ensure a comprehensive comparison, covering both advanced DE variants and non-DE-based optimization techniques and their default parameter settings are given in Table 1. The six PEMFC test systems used in this study included BCS 500 W, Nedstack 600 W PS6, SR-12 W, Horizon H-12, Ballard Mark V, and STD 250 W. These stacks represented a diverse range of operational characteristics as mentioned in Table 2, to assess the generalizability and adaptability of PCM-DE. The performance metrics included the best, worst, mean SSE values, and standard deviation (STD) across 40 independent runs for each algorithm. Overall, PCM-DE demonstrated faster convergence, lower SSE values, and improved robustness, especially under the nonlinear and complex operational conditions of PEMFC stacks. These results underscore its potential to enhance the precision and reliability of PEMFC parameter identification, establishing a foundation for further exploration into dynamic operating conditions and broader applications in sustainable energy systems.

Case 1: BCS 500 W PEMFC optimization

To evaluate the efficacy of the proposed PCM-DE algorithm, the BCS 500 W PEMFC stack was used as the first case study. This system comprises 32 cells, an active area of $A = 64\text{cm}^2$, a membrane thickness of $l = 178\mu\text{m}$, and operates at a temperature of $T = 333\text{K}$ under specific partial pressures of hydrogen ($P_{\text{H}_2} = 1.0\text{bar}$) and oxygen ($P_{\text{O}_2} = 0.2095\text{bar}$). The performance of PCM-DE was compared against nine state-of-the-art algorithms, namely TDE, PSO-sono, CS-DE, jSO, EDO, LSHADE, HSES, E-QUATRE, and EA4eig, over 40 independent runs. The optimization aimed to minimize the Sum of Squared Error (SSE), with results summarized in Table 3. The optimal parameter values ($\xi_1, \xi_2, \xi_3, \xi_4, \lambda, R_c, \text{and } B$) estimated by PCM-DE and the comparison algorithms are presented in Table 3. PCM-DE demonstrated superior accuracy with values aligning closely with the experimental data. Specifically, the optimal value for ξ_1 identified by PCM-DE was -0.85335, which is notably

Algorithm	TDE	PSO-sono	CS-DE	jSO	EDO	LSHADE	HSES	E-QUATRE	EA4eig	PCM-DE
ξ_1	−0.95401	−0.89978	−1.15843	−1.08142	−0.85419	−0.90586	−0.85633	−1.01163	−1.0893	−0.85335
ξ_2	0.003313	0.002668	0.003321	0.003445	0.002726	0.003285	0.002504	0.003498	0.003411	0.002508
ξ_3	8.89E−05	5.84E−05	5.04E−05	7.33E−05	7.09E−05	9.69E−05	5.62E−05	9.02E−05	6.98E−05	5.71E−05
ξ_4	−0.0002	−0.00019	−0.00019	−0.00019	−0.00019	−0.00019	−0.00019	−0.00019	−0.00018	−0.00019
λ	22.94007	22.81753	20.87724	21.4162	22.66794	22.39264	21.06737	20.89538	22.04643	20.87724
R_c	0.000208	0.000309	0.0001	0.000229	0.000264	0.000226	0.000134	0.0001	0.0008	0.0001
B	0.015165	0.01605	0.016126	0.01579	0.016178	0.016214	0.015978	0.016135	0.0136	0.016126
$Min\ SSE$	0.048204	0.025774	0.025493	0.02608	0.025649	0.026159	0.025626	0.025494	0.048119	0.025493
$Max\ SSE$	0.152459	0.039238	0.041017	0.039675	0.027453	0.03673	0.026337	0.025549	0.251904	0.025653
$Mean\ SSE$	0.094939	0.031254	0.030638	0.030274	0.026156	0.029913	0.025911	0.025521	0.123943	0.025525
$S.D.$	0.046433	0.006924	0.007229	0.005797	0.000738	0.004328	0.000324	2.34E−05	0.080178	7.16E−05
$R.T.$	3.443282	3.174415	2.694598	2.772529	6.007913	6.51895	5.140466	5.926041	8.458082	0.347238
$F.R.$	9.4	6.6	4.8	6.4	4.6	6.4	3.8	2	9.6	1.4

Table 3. Optimal parameters and performance metrics for BCS 500 W PEMFC parameter identification using PCM-DE and comparative algorithms.

consistent with the physical characteristics of the fuel cell. Similarly, other parameters, including $\xi_2 = 0.002508$ and $\xi_3 = 5.71 \times 10^{-5}$, exhibited high precision, outperforming alternative algorithms. Notably, the parameters $R_c = 0.0001$ and $B = 0.016126$ further confirm the robustness of PCM-DE in achieving optimal values within the expected ranges. The minimum, maximum, and mean SSE values provide a comprehensive assessment of the algorithm's performance. PCM-DE achieved the lowest mean SSE (0.025525) and minimum SSE (0.025493), outperforming all competing algorithms. For instance, the closest competitors, CS-DE and E-QUATRE, had slightly higher mean SSE values of 0.030638 and 0.025521, respectively. In terms of maximum SSE, PCM-DE maintained a narrow range (0.025653), demonstrating exceptional stability compared to algorithms such as TDE (0.152459) and EA4eig (0.251904).

The standard deviation ($S.D.$) further highlights PCM-DE's robustness, achieving the lowest $S.D.$ value (7.16×10^{-5}), which reflects minimal variability across runs. This is a significant improvement compared to other -DE significantly reduced computational time, achieving the fastest runtime ($R.T. = 0.347238$s), which is a substantial improvement compared to the other algorithms. The second-best runtime was observed with CS-DE (2.694598s), while LSHADE (6.51895s) and EA4eig (8.458082s) required considerably longer execution times.

The performance of PCM-DE is further supported by graphical evaluations shown in Fig. 3. The estimated I/V and P/V curves using PCM-DE parameters closely match the experimentally measured values, demonstrating the algorithm's accuracy in parameter estimation. This indicates a high degree of correlation between algorithms, such as TDE (0.046433) and PSO-sono (0.006924). PCM-DE's performance also aligns with its superior Friedman Ranking (1.4), indicating consistent and robust optimization results. Additionally, PCMthe estimated and measured data across all current values. Absolute error (AE) and relative error (RE) remain consistently low for PCM-DE across the operating current range. The RE remains below 1%, with AE showing minimal deviations, confirming PCM-DE's superior precision. The box plot illustrates PCM-DE's tight distribution of fitness values with negligible outliers, further reinforcing its robustness compared to other algorithms such as TDE and EA4eig, which show wider variability. The convergence curve reveals that PCM-DE rapidly converges to the global optimum within the first 50 iterations. In contrast, other algorithms such as TDE and PSO-sono exhibit slower convergence and higher fitness values throughout the iterations.

Case 2: Nedstack 600 W PS6 optimization

The Nedstack 600 W PS6 PEMFC was employed to evaluate the performance of the proposed PCM-DE algorithm in comparison to nine other advanced optimization algorithms. The optimal parameter values and associated SSE for each algorithm are presented in Table 4. PCM-DE outperformed all other algorithms by achieving the lowest SSE value of 0.275211 across 40 independent runs, reflecting its superior parameter estimation accuracy. Notably, PCM-DE demonstrated remarkable consistency, as evidenced by a standard deviation (Std.) of 3.54×10^{-16}, the smallest among all algorithms, confirming its robustness.

The boxplot in Fig. 4b further substantiates the competitive performance of PCM-DE, showcasing a narrow variance compared to competing methods like TDE and EA4eig, which exhibited higher SSE dispersion. The convergence behavior of PCM-DE is illustrated in Fig. 4c, indicating rapid minimization of the objective function within 50 iterations, far surpassing the performance of TDE, PSO-sono, and other competitors. This highlights PCM-DE's efficient exploration and exploitation capabilities in identifying optimal parameters for the fuel cell model. In Fig. 4a, the estimated I–V and P-V curves closely align with the measured values, demonstrating PCM-DE's ability to generate a high-fidelity PEMFC model. The absolute error (AE) and relative error (RE%) plots emphasize minimal deviations, with absolute error values generally remaining below 0.2, reinforcing the precision of PCM-DE's parameter estimation. Collectively, these results confirm PCM-DE as a robust and precise method for PEMFC parameter optimization under varying conditions.

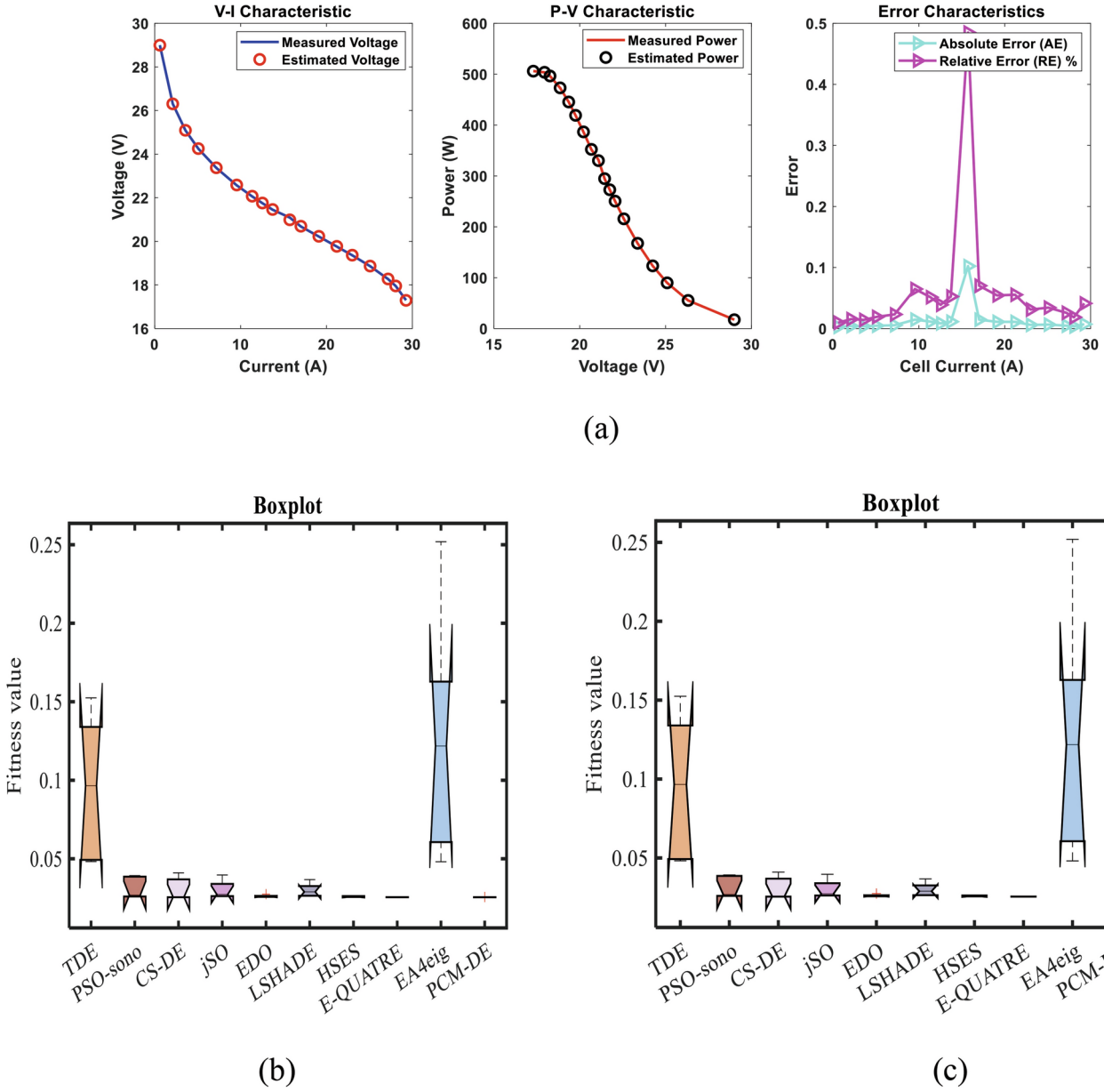

Fig. 3. (**a**) I–V and P–V characteristics with error metrics for BCS 500 W PEMFC; (**b**) SSE distribution boxplot; (**c**) Convergence curves comparing PCM-DE with other algorithms.

Case 3: SR-12 W PEMFC optimization

The SR-12 W fuel cell stack was employed to validate the efficacy of the PCM-DE algorithm against alternative optimization methods. The evaluated algorithms, including TDE, PSO-sono, CS-DE, jSO, EDO, LSHADE, HSES, E-QUATRE, EA4eig, and PCM-DE, were run across 40 iterations. Table 5 presents the optimal parameter values (ξ_1, ξ_2, ξ_3, ξ_4, λ, R_c, and B), SSE metrics, and statistical performance indicators for each algorithm. PCM-DE outperformed its competitors with the lowest Min. SSE (0.242284) and Mean SSE (0.242413), alongside a near-negligible standard deviation (S.D. $= 0.000288$), indicating high robustness and accuracy. The computational runtime for PCM-DE was significantly reduced (R.T. $= 0.191303$ seconds) compared to the prolonged execution times of TDE and EA4eig, which exhibited R.T. values of 3.302317 and 6.616477 s, respectively. Furthermore, PCM-DE secured the lowest Friedman Ranking (F.R. $= 2.2$), underscoring its superior convergence reliability.

The graphical insights in Fig. 5a–c corroborate these findings. The $I - V$ and $P - V$ characteristics (Fig. 5a) illustrate an exceptional fit between the measured and estimated performance curves. Minimal deviations were observed in the Error Characteristics (Fig. 5a), as evident from the Absolute Error (AE) and Relative Error (RE) plots, which remained consistently low across all current levels. The boxplot in Fig. 5b further highlights PCM-DE's narrower fitness value distribution compared to other algorithms, affirming its robustness in parameter

Algorithm	TDE	PSO-sono	CS-DE	jSO	EDO	LSHADE	HSES	E-QUATRE	EA4eig	PCM-DE
ξ_1	−0.8532	−0.85326	−1.08913	−0.86358	−0.92348	−1.01337	−1.17905	−1.0535	−1.15774	−0.8532
ξ_2	0.002526	0.002412	0.003474	0.002596	0.002949	0.002922	0.003959	0.003407	0.003619	0.002398
ξ_3	4.46E−05	3.69E−05	6.37E−05	4.79E−05	6.05E−05	4E−05	7.96E−05	6.63E−05	5.99E−05	3.6E−05
ξ_4	−9.8E−05	−9.5E−05	−9.5E−05	−9.5E−05	−9.6E−05	−9.5E−05	−9.5E−05	−9.5E−05	−9.7E−05	−9.5E−05
λ	17.43809	14	14	14.00098	14.09997	14	14	14.0015	14	14
R_c	0.000151	0.000138	0.00012	0.000123	0.000138	0.000127	0.000127	0.000116	0.000106	0.00012
B	0.039693	0.014355	0.016788	0.01667	0.015466	0.015974	0.015901	0.017471	0.0136	0.016788
$MinSSE$	0.305819	0.275707	0.275211	0.275295	0.277726	0.275275	0.275279	0.275558	0.32006	0.275211
$MaxSSE$	0.48555	0.295151	0.276061	0.276252	0.288212	0.30399	0.276239	0.285524	0.694938	0.275211
$MeanSSE$	0.366083	0.285689	0.275826	0.275706	0.283945	0.28706	0.275925	0.280497	0.481343	0.275211
$S.D.$	0.072061	0.007078	0.000354	0.000397	0.003835	0.012318	0.000375	0.00401	0.174857	3.54E−16
$R.T.$	4.188091	4.680892	5.20477	5.637507	12.09401	5.273439	5.490955	5.421907	10.72658	0.313721
$F.R.$	9.4	6.6	3.4	3.2	6.6	6	4	5.2	9.6	1

Table 4. Optimal parameters and performance metrics for Nedstack 600 W PS6 PEMFC parameter identification using PCM-DE and comparative algorithms.

identification. Lastly, the convergence curve (Fig. 5c) confirms PCM-DE's rapid descent toward optimality, stabilizing after a minimal number of iterations.

Case 4: Horizon H-12 PEMFC optimization

The Horizon H-12 PEMFC stack was selected to examine the robustness of the PCM-DE algorithm in parameter estimation, contrasting its performance with TDE, PSO-sono, CS-DE, jSO, EDO, LSHADE, HSES, E-QUATRE, and EA4eig algorithms. The comparison across 40 independent runs highlighted PCM-DE's distinct advantages. Table 6 details the optimal parameters (ξ_1, ξ_2, ξ_3, ξ_4, λ, R_c, and B), SSE values, and statistical metrics obtained for each algorithm. PCM-DE achieved the lowest $\mathrm{Min.\ SSE}$ (0.102915) and $\mathrm{Mean\ SSE}$ (0.102915), with negligible variability ($\mathrm{S.D.} = 1.08 \times 10^{-16}$), signifying its exceptional precision and consistency. In terms of computational efficiency, PCM-DE delivered the shortest runtime ($\mathrm{R.T.} = 0.179717$ seconds), significantly outperforming EA4eig ($\mathrm{R.T.} = 6.434734$) and TDE ($\mathrm{R.T.} = 3.258615$). Moreover, the Friedman Ranking ($\mathrm{F.R.} = 1.2$) substantiates PCM-DE's superiority over all competitors, demonstrating optimal convergence capabilities.

The graphical representations in Fig. 6a–c support these observations. The $I - V$ and $P - V$ characteristics (Fig. 6a) illustrate a near-perfect alignment between the measured and estimated values, confirming the accuracy of PCM-DE in modeling the fuel cell behavior. Figure 6a shows that the Error Characteristics are minimally deviated from zero, with both Absolute Error ("AE") and Relative Error ("RE") staying low over all current densities. Figure 6b also shows that PCM-DE has robust performance, as its fitness value distribution is more compact than other algorithms. Moreover, the convergence curve (Fig. 6c) illustrates that PCM-DE converges to the global optimum at a much faster rate than the other methods using a small number of iterations.

In summary, PCM-DE is found to be remarkably accurate, robust and computationally efficient in estimating the parameters of the Horizon H-12 PEMFC stack and is therefore effective and reliable for low power fuel cell applications.

Case 5: Ballard Mark V PEMFC optimization

The parameter optimization for the Ballard Mark V PEMFC stack was conducted to evaluate the robustness and accuracy of the PCM-DE algorithm compared to other state-of-the-art algorithms, namely TDE, PSO-sono, CS-DE, jSO, EDO, LSHADE, HSES, E-QUATRE, and EA4eig. Key results, including optimal parameter values and performance metrics, are summarized in Table 7.

The PCM-DE algorithm exhibited the smallest minimum SSE value of 0.148632, outperforming all competing algorithms. The mean SSE was also the lowest for PCM-DE, highlighting its accuracy and precision in modeling the Ballard Mark V stack. The algorithm demonstrated remarkable stability, evidenced by its negligible standard deviation (4.25×10^{-16}). Furthermore, PCM-DE achieved the fastest runtime (0.212878s), significantly surpassing other algorithms. Figure 7a presents the I–V and P–V characteristic curves, where the optimized parameters produced a close fit between the estimated and experimental data, confirming the model's reliability. Error analysis in the same figure highlights the minimal absolute error (AE) and relative error (RE%), which were consistently low across the current range. Figure 7b depicts the box plot of fitness values, underscoring the superior performance and lower dispersion of PCM-DE compared to other algorithms. Finally, the convergence curve in Fig. 7c shows PCM-DE's rapid convergence to the optimal solution within the first few iterations, outperforming the other algorithms in terms of speed and accuracy.

Case 6: STD 250 W Stack PEMFC optimization

The performance of the proposed PCM-DE algorithm was benchmarked against nine other advanced optimization algorithms using the CASE 6 STD 250 W stack PEMFC. The optimal parameter values and associated statistical metrics for each algorithm are summarized in Table 8. PCM-DE demonstrated outstanding

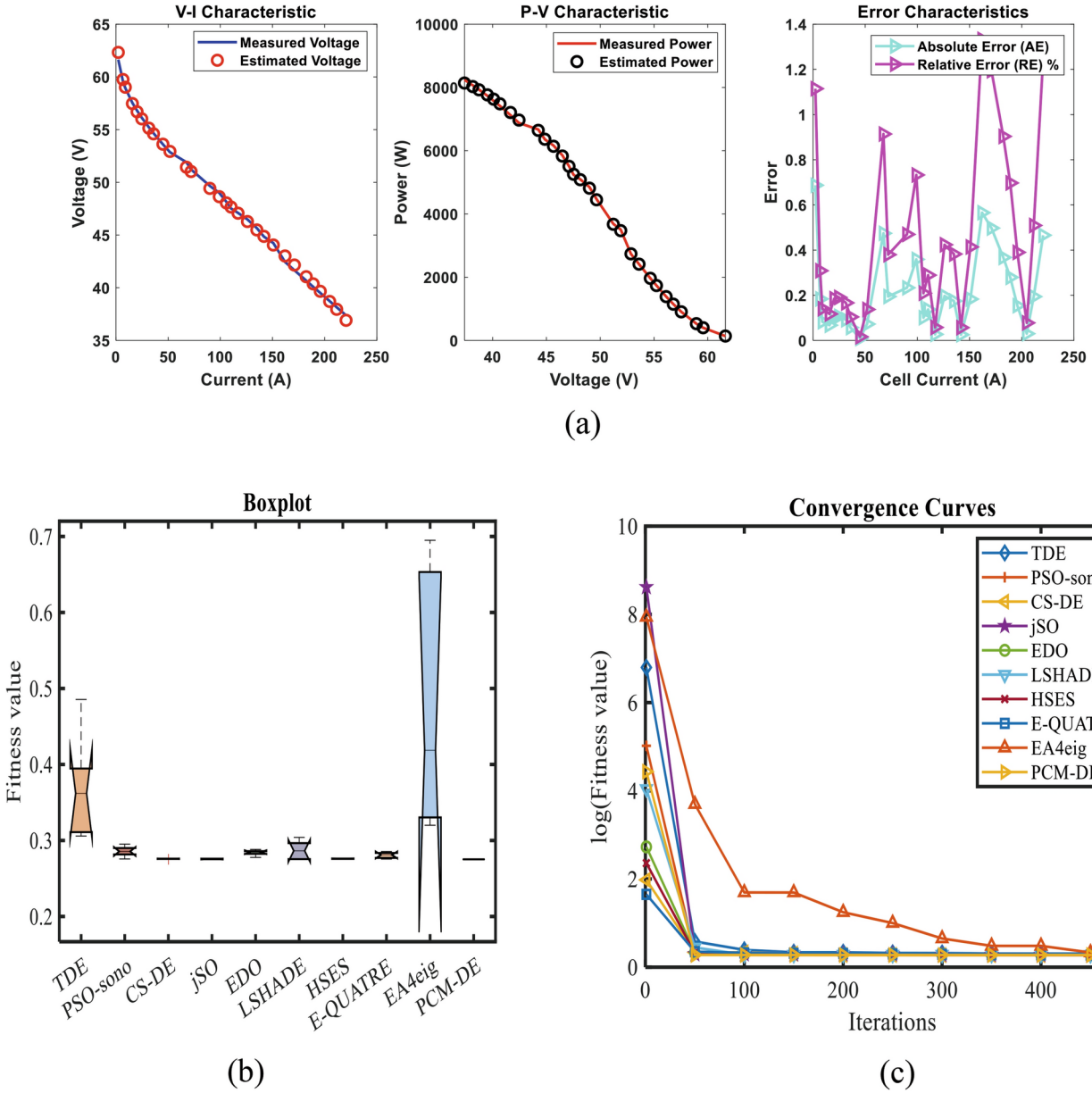

Fig. 4. (**a**) I–V and P–V characteristics with error metrics for Nedstack 600 W PS6 PEMFC; (**b**) SSE distribution boxplot; (**c**) Convergence curves comparing PCM-DE with other algorithms.

performance by achieving a mean SSE value of 0.283774, which matched the best-performing algorithms such as CS-DE, LSHADE, and E-QUATRE. The minimal standard deviation (S.D.) of PCM-DE, at 2.15×10^{-16}, highlights its remarkable consistency across runs, significantly outperforming competitors like LSHADE (1.81×10^{-2}) and EA4eig (3.36×10^{-2}), which exhibited much larger deviations. PCM-DE also demonstrated highly efficient computation, evidenced by the shortest recorded runtime (R.T.) of 0.219201 s, far surpassing the runtimes of other algorithms such as EA4eig (5.55041 s) and EDO (5.310678 s). Furthermore, the failure rate (F.R.) of PCM-DE was the lowest among all algorithms, at 1, indicating its exceptional reliability in consistently finding optimal solutions.

Examining the physical parameters, PCM-DE achieved accurate estimations for critical values such as ξ_1, ξ_2, ξ_3, and λ. For example, PCM-DE's estimation for ξ_1 was −1.14613, closely aligned with other leading methods but demonstrating a superior trade-off between precision and robustness. Similarly, PCM-DE yielded the lowest residual value for R_a (0.000557), which is a critical parameter for the PEMFC model, underscoring its high precision in capturing the physical characteristics of the fuel cell. Further substantiation of the stability of PCM-DE is provided by its narrow range of Min SSE (0.283774) and Max SSE (0.283774), which demonstrates excellent repeatability. This is a strikingly different performance to methods such as EA4eig which had a greater range of SSE values, indicative of a less consistent performance.

Algorithm	TDE	PSO-sono	CS-DE	jSO	EDO	LSHADE	HSES	E-QUATRE	EA4eig	PCM-DE
ξ_1	−1.17309	−1.00669	−1.09789	−1.10324	−0.99069	−1.18998	−0.95623	−1.07929	−0.90673	−1.17676
ξ_2	0.003927	0.003722	0.003746	0.003199	0.003038	0.00357	0.003209	0.003544	0.002544	0.003878
ξ_3	7.82E−05	9.79E−05	8.1E−05	4.47E−05	5.7E−05	5.14E−05	7.49E−05	7.19E−05	4.04E−05	7.4E−05
ξ_4	−9.6E−05	−9.5E−05	−9.5E−05	−9.6E−05	−9.5E−05	−9.6E−05	−9.5E−05	−9.5E−05	−0.00011	−9.5E−05
λ	23	22.99978	23	20.56372	22.58277	22.84515	21.54319	22.69353	14.44028	23
R_c	0.000114	0.000629	0.0008	0.000648	0.000675	0.000631	0.000683	0.000665	0.000505	0.000673
B	0.187339	0.176187	0.172796	0.17516	0.175088	0.175452	0.174676	0.175466	0.169446	0.17532
$MinSSE$	0.251538	0.242335	0.242716	0.242544	0.242312	0.242653	0.242392	0.242312	0.288483	0.242284
$MaxSSE$	0.503904	0.243855	0.242927	0.245857	0.243975	0.246359	0.242456	0.242465	0.720728	0.242927
$MeanSSE$	0.319768	0.243012	0.242801	0.244256	0.242855	0.244126	0.242417	0.242392	0.403134	0.242413
$S.D.$	0.105035	0.000545	0.000116	0.001524	0.000675	0.001421	2.41E−05	6.65E−05	0.180209	0.000288
$R.T.$	3.302317	3.586536	3.203986	3.265841	6.366491	4.927801	5.140807	5.182792	6.616477	0.191303
$F.R.$	9.2	5.6	5.2	6.8	4.4	6.8	2.8	2.2	9.8	2.2

Table 5. Optimal parameters and performance metrics for SR-12 W PEMFC parameter identification using PCM-DE and comparative algorithms.

Figure 8 also shows the effectiveness of PCM-DE. The alignment of the estimated I–V and P–V curves with the measured data in Fig. 8a confirms PCM-DE's capability of producing a high fidelity PEMFC model. The plots of absolute error (AE) and relative error (RE%) are almost constant and demonstrate the precision and robustness of PCM-DE's parameter estimation. Figure 8b shows that PCM-DE has minimal variance compared to other algorithms such as TDE and EA4eig, which had wider dispersions. This demonstrates that PCM-DE is on par with itself across multiple runs. As shown in Fig. 8c, the convergence plot shows that PCM-DE converged in less than 50 iterations, faster than all other algorithms in terms of optimization speed. PCM-DE shows rapid convergence, which shows its ability to balance exploration and exploitation, to quickly and accurately estimate parameters.

Conclusion

A novel Differential Evolution based optimization algorithm, PCM-DE, for accurate parameter identification of Proton Exchange Membrane Fuel Cells (PEMFCs) was presented. By combining a perturbation mechanism, a covariance matrix based stagnation indicator, and a two phase parameter adaptation strategy, PCM-DE showed better accuracy, robustness, speed of convergence, and computational efficiency. The key findings, their significance, reservations, and limitations of the study are summarized in this section, and an outlook for future research directions is provided.

Key findings

Several important findings were found from the performance analysis of PCM-DE in PEMFC parameter estimation. In all six PEMFC stacks, PCM-DE had the lowest minimum Sum of Squared Errors (SSE), demonstrating the highest accuracy among state of the art algorithms. For instance, PCM-DE achieved SSE values of 0.025493 for the BCS 500 W stack and 0.102915 for the Horizon H-12 stack, which are lower than those of the competing algorithms TDE, PSO-sono, and CS-DE. Furthermore, PCM-DE proved to be reliable with low standard deviations in SSE, with 3.54E−16 for the Nedstack 600 W PS6 stack and 2.15E−16 for the STD 250 W stack. In addition, the convergence analysis showed that PCM-DE can reach the optimal solutions in much fewer iterations than other algorithms, which is illustrated by the fast convergence curves. PCM-DE is shown to have the potential to improve the precision and reliability of PEMFC modeling.

Significance

Innovations in PCM-DE overcome several longstanding issues that exist in optimization of PEMFC parameter estimation, including premature convergence, population stagnation, and inefficient exploration of the search space. It demonstrates its adaptability to different operational conditions by showing robust performance across a range of PEMFC stacks, including high power configurations such as the Ballard Mark V (5000 W) and low power systems such as the Horizon H-12 (12 W). The high computational efficiency of PCM-DE, with runtime values as low as 0.179717 s for the Horizon H-12 stack, indicates that PCM-DE may be used for real time applications in energy systems. The ability of the algorithm to accurately model PEMFCs can serve as the basis for further development of sustainable energy technologies and the more widespread use of hydrogen fuel cells.

Reservations and limitations

However, the performance of PCM-DE under dynamic and transient PEMFC operational conditions is not yet examined. In addition, PEMFCs used in practice generally run under specific load demands and environmental conditions that may adversely affect the algorithm. Furthermore, further study is needed to determine the scalability of PCM-DE to larger PEMFC stacks or more complex, high dimensional optimization problems. A second limitation is that this study does not consider multi-objective optimization scenarios, which are necessary

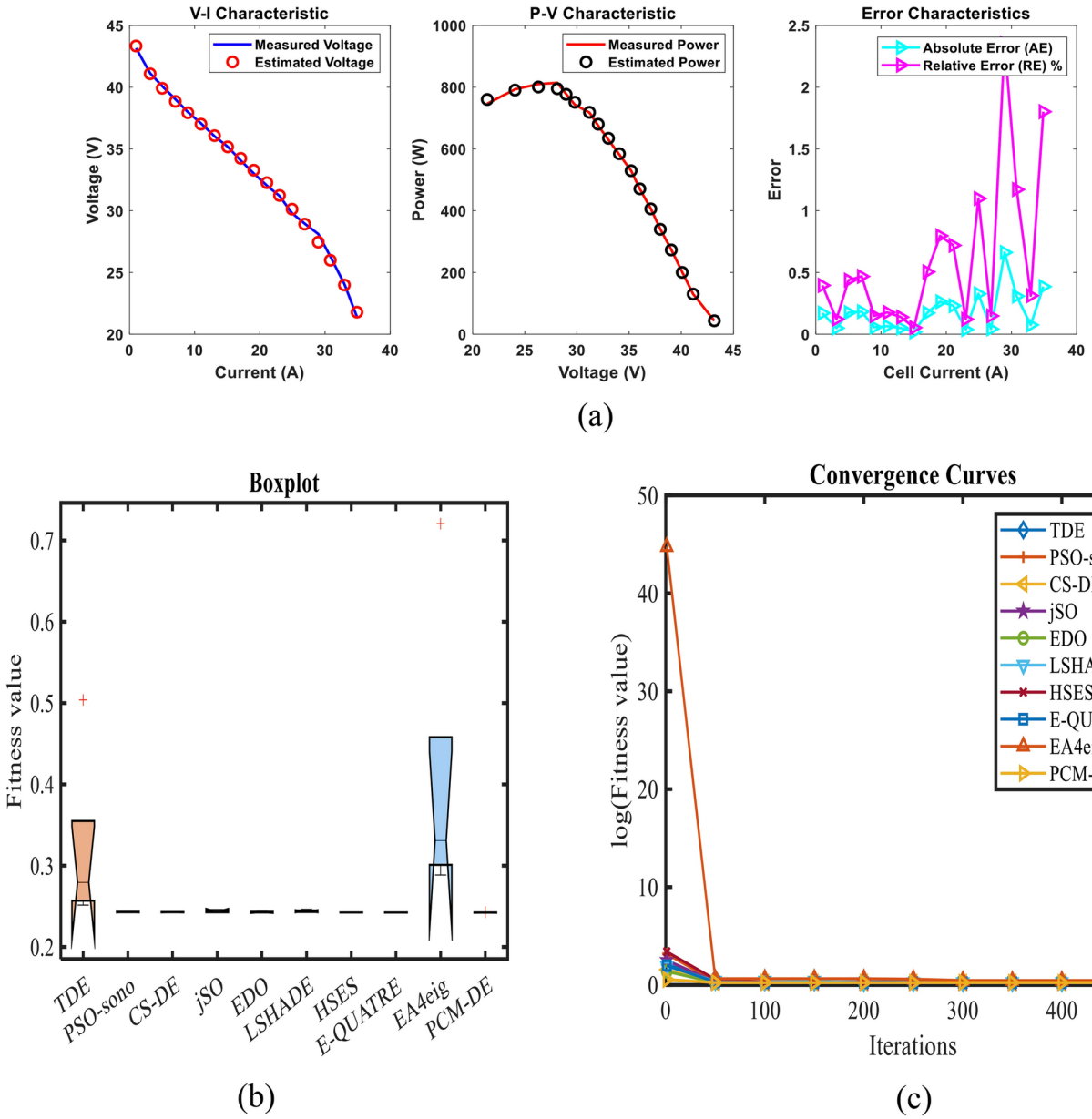

Fig. 5. (**a**) I–V and P–V characteristics with error metrics for SR-12 W PEMFC; (**b**) SSE distribution boxplot; (**c**) Convergence curves comparing PCM-DE with other algorithms.

to trade off between conflicting design criteria in real systems. Overcoming these limitations will increase PCM-DE's applicability and effectiveness in wider energy system contexts.

Future directions

Future research should extend PCM-DE's capabilities to dynamic PEMFC environments with varying operating conditions such as temperature, pressure and load current in real time. Investigations of this type will allow us to understand the extent of PCM-DE's flexibility and robustness under realistic conditions. Furthermore, PCM-DE can be hybridized with other algorithms to solve multi objective optimization problems involving tradeoffs between objectives such as efficiency, durability and cost. Beyond this, PCM-DE's potential to optimize other clean energy technologies, including Solid Oxide Fuel Cells or hybrid renewable energy systems, will be explored. Finally, we will further refine PCM-DE's computational framework to improve its scalability and reduce resource consumption for large scale optimization tasks so that it can be adopted for industrial and commercial applications.

In conclusion, PCM-DE is a major improvement in PEMFC parameter estimation that provides a robust and efficient method for improving fuel cell performance and reliability. New avenues for advancing clean energy technologies and fostering sustainable development are opened by its potential application to dynamic and multi-objective optimization scenarios.

Algorithm	TDE	PSO-sono	CS-DE	jSO	EDO	LSHADE	HSES	E-QUATRE	EA4eig	PCM-DE
ξ_1	− 0.8532	− 0.8532	− 0.8532	− 1.06956	− 1.04521	− 1.0951	− 1.09132	− 0.85663	− 0.8532	− 0.87423
ξ_2	0.002222	0.001509	0.001947	0.00268	0.002208	0.002896	0.002599	0.001823	0.001878	0.001596
ξ_3	8.72E−05	0.000036	6.75E−05	7.21E−05	4.36E−05	8.19E−05	6.14E−05	5.78E−05	6.26E−05	3.76E−05
ξ_4	− 0.00011	− 0.00011	− 0.00011	− 0.00011	− 0.00011	− 0.00011	− 0.00011	− 0.00011	− 0.00011	− 0.00011
λ	14	14	14	14.05657	14.00008	14.12929	14	14.00101	14.88267	14
R_c	0.0008	0.0008	0.0008	0.000396	0.0008	0.00075	0.0008	0.0008	0.000312	0.0008
B	0.0136	0.0136	0.0136	0.01365	0.013607	0.013605	0.0136	0.0136	0.013926	0.0136
$MinSSE$	0.102915	0.102915	0.102915	0.103355	0.102916	0.103004	0.102915	0.102916	0.103721	0.102915
$MaxSSE$	0.106373	0.103641	0.104428	0.103608	0.103195	0.104928	0.102916	0.102926	0.116115	0.102915
$MeanSSE$	0.104707	0.103151	0.103363	0.103508	0.10299	0.103738	0.102915	0.102919	0.107378	0.102915
$S.D.$	0.001711	0.000337	0.000673	9.61E−05	0.000119	0.00077	5.38E−07	4.04E−06	0.005077	1.08E−16
$R.T.$	3.258615	3.299494	3.11348	3.675928	6.406508	3.637585	3.752429	4.412898	6.434734	0.179717
$F.R.$	7	4.8	4.4	7	5.6	7	3.4	4.6	10	1.2

Table 6. Optimal parameters and performance metrics for Horizon H-12 PEMFC parameter identification using PCM-DE and comparative algorithms.

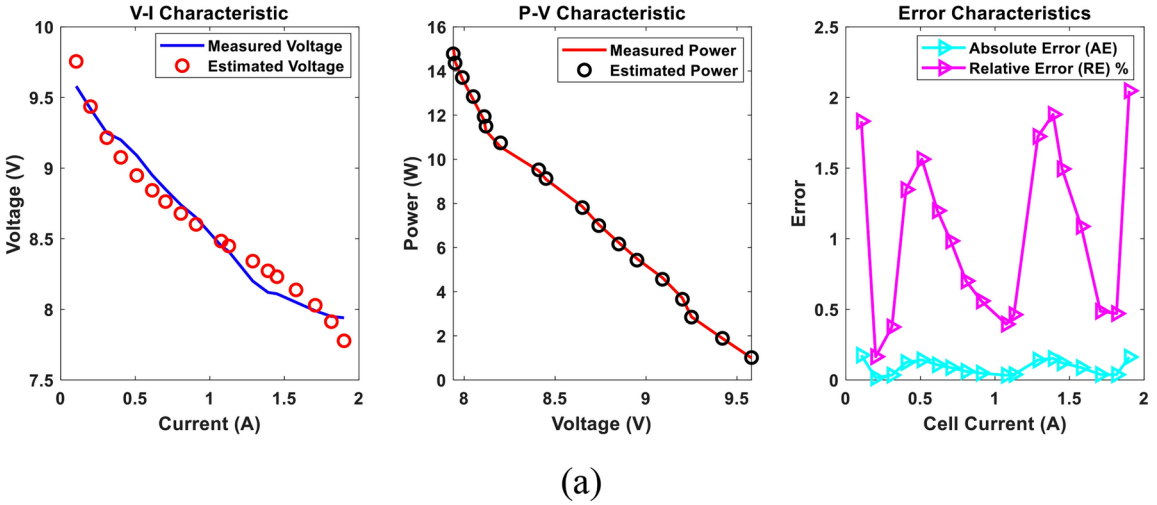

(a)

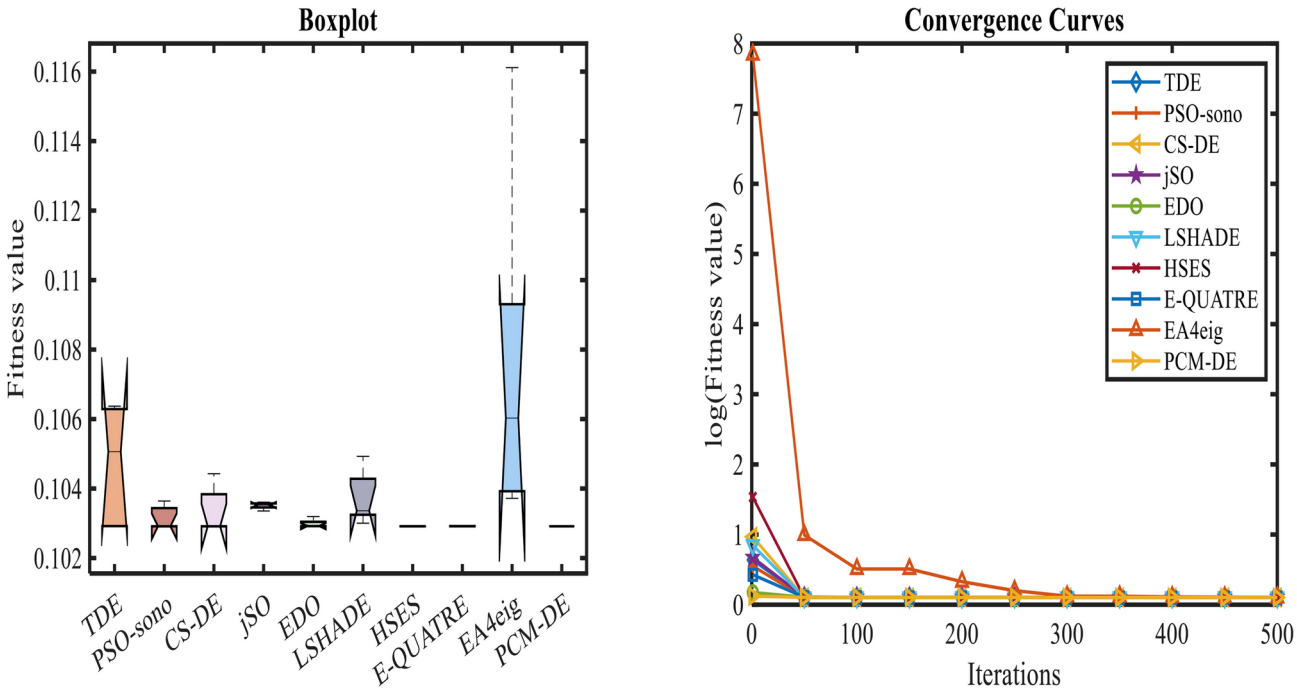

(b) (c)

Fig. 6. (**a**) I–V and P–V characteristics with error metrics for Horizon H-12 PEMFC; (**b**) SSE distribution boxplot; (**c**) Convergence curves comparing PCM-DE with other algorithms.

Algorithm	TDE	PSO-sono	CS-DE	jSO	EDO	LSHADE	HSES	E-QUATRE	EA4eig	PCM-DE
ξ_1	− 0.9046	− 1.02447	− 0.8532	− 1.16458	− 1.07675	− 0.88563	− 1.09596	− 1.1182	− 1.04378	− 1.00257
ξ_2	0.002561	0.003136	0.003108	0.003631	0.003694	0.002541	0.003597	0.003431	0.003354	0.002829
ξ_3	4.67E−05	6.3E−05	9.66E−05	6.91E−05	9.19E−05	4.95E−05	8.1E−05	6.45E−05	7.47E−05	4.56E−05
ξ_4	− 0.00017	− 0.00017	− 0.00017	− 0.00017	− 0.00017	− 0.00017	− 0.00017	− 0.00017	− 0.00018	− 0.00017
λ	16.20935	14.55353	14.35531	14.62292	14.49033	14.95144	14.46494	14.46515	19.189	14.43913
R_c	0.0008	0.000215	0.0001	0.000197	0.000116	0.000287	0.0001	0.0001	0.000411	0.0001
B	0.014194	0.01371	0.0136	0.01364	0.013803	0.014034	0.013747	0.013848	0.020392	0.013795
$MinSSE$	0.149801	0.148846	0.148643	0.148835	0.148662	0.149023	0.148682	0.148634	0.161378	0.148632
$MaxSSE$	0.18154	0.151037	0.14973	0.156704	0.149227	0.151692	0.148904	0.148642	0.230197	0.148632
$MeanSSE$	0.161807	0.149751	0.149176	0.151331	0.148979	0.149808	0.148783	0.148638	0.179607	0.148632
$S.D.$	0.011782	0.00087	0.000502	0.003137	0.000271	0.001136	9.13E−05	3.13E−06	0.028525	4.25E−16
$R.T.$	2.844662	3.194451	2.539139	2.593499	5.596922	3.278105	3.464875	3.827038	5.804909	0.212878
$F.R.$	8.8	6.4	4.8	7.2	5.2	5.8	4	2	9.8	1

Table 7. Optimal parameters and performance metrics for Ballard Mark V PEMFC parameter identification using PCM-DE and comparative algorithms.

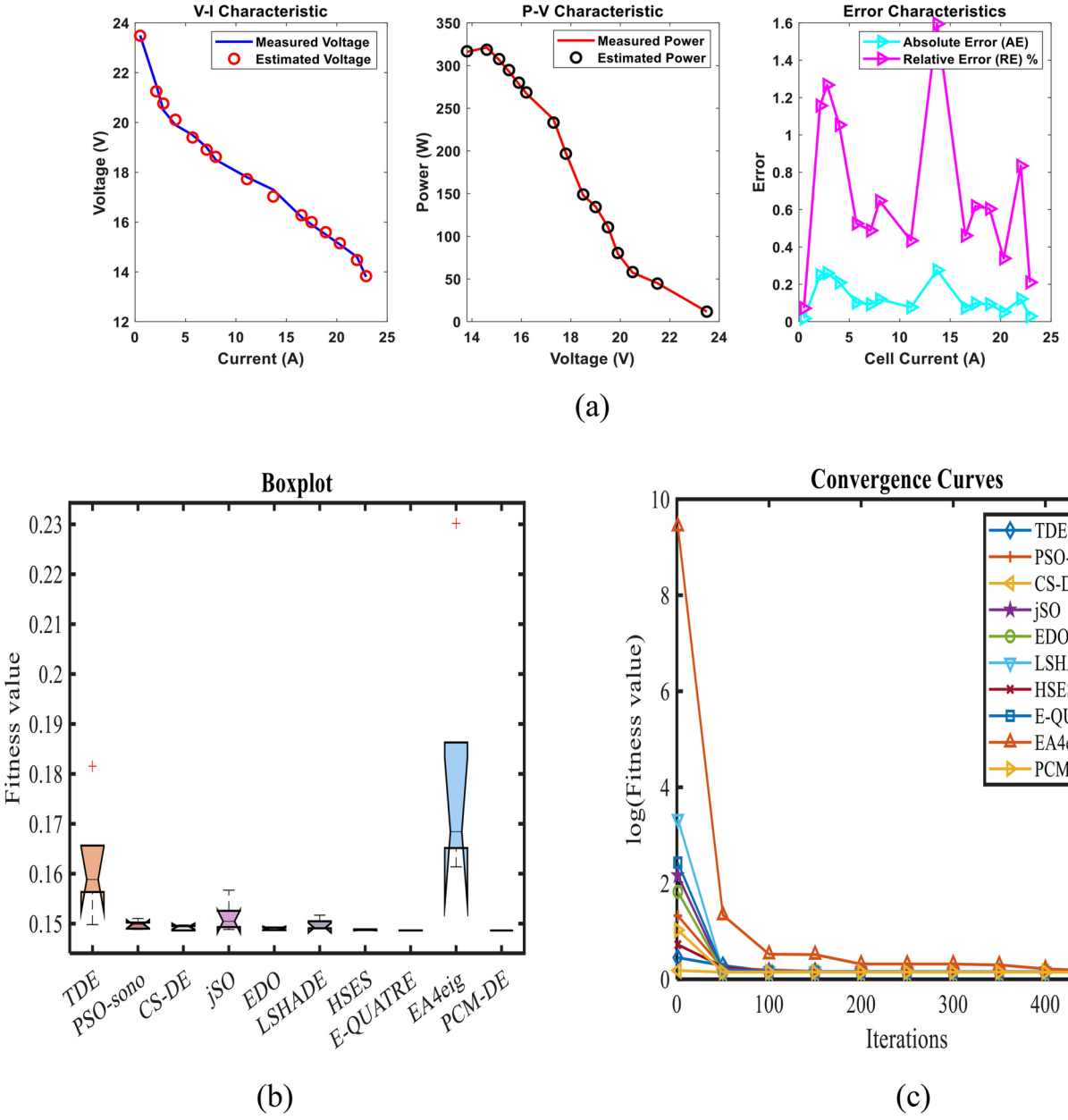

Fig. 7. (**a**) I–V and P–V characteristics with error metrics for Ballard Mark V PEMFC; (**b**) SSE distribution boxplot; (**c**) Convergence curves comparing PCM-DE with other algorithms.

Algorithm	TDE	PSO-sono	CS-DE	jSO	EDO	LSHADE	HSES	E-QUATRE	EA4eig	PCM-DE
ξ_1	− 1.11731	− 0.85321	− 1.19969	− 1.13797	− 1.05217	− 0.8532	− 0.98167	− 0.93878	− 1.14613	− 0.86664
ξ_2	0.003091	0.002025	0.002902	0.002793	0.002897	0.001964	0.002995	0.002597	0.002771	0.001939
ξ_3	6.8E−05	4.66E−05	0.000036	4.14E−05	6.69E−05	4.22E−05	8.87E−05	6.94E−05	3.72E−05	3.76E−05
ξ_4	− 0.00016	− 0.00017	− 0.00017	− 0.00017	− 0.00017	− 0.00017	− 0.00017	− 0.00017	− 0.00018	− 0.00017
λ	14	14	14	14.09223	14	15.38946	14	14.00067	14.14164	14
R_c	0.0008	0.0008	0.0008	0.0008	0.0008	0.0008	0.0008	0.0008	0.000557	0.0008
B	0.018466	0.017317	0.017317	0.017261	0.01731	0.017817	0.017312	0.017329	0.016022	0.017317
$MinSSE$	0.293033	0.283774	0.283774	0.284081	0.283774	0.287924	0.28379	0.283778	0.315181	0.283774
$MaxSSE$	0.324045	0.283775	0.283774	0.320353	0.283809	0.330113	0.2839	0.283884	0.400246	0.283774
$MeanSSE$	0.307293	0.283774	0.283774	0.300414	0.283786	0.318682	0.283834	0.283809	0.343238	0.283774
$S.D.$	0.014954	4.2E−07	3.05E−16	0.017809	1.58E−05	0.018076	4.88E−05	4.39E−05	0.033639	2.15E−16
$R.T.$	2.903845	2.978546	2.351964	2.914248	5.310678	3.386743	4.633986	3.934403	5.55041	0.219201
$F.R.$	7.8	3.2	2	7.8	4.2	8.6	5.6	5	9.8	1

Table 8. Optimal parameters and performance metrics for STD 250 W stack PEMFC parameter identification using PCM-DE and comparative algorithms.

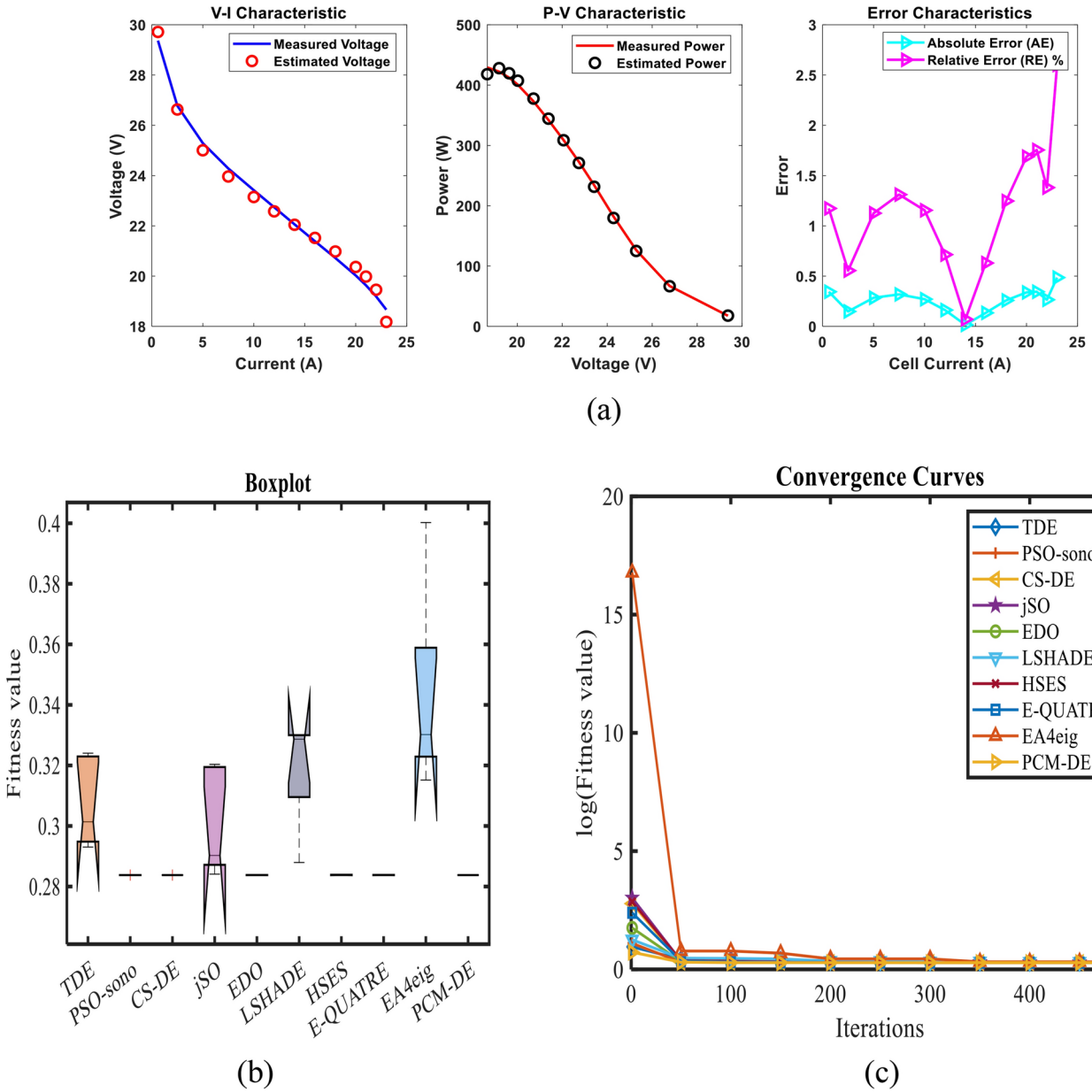

Fig. 8. (**a**) I–V and P–V characteristics with error metrics for STD 250 W Stack PEMFC; (**b**) SSE distribution boxplot; (**c**) Convergence curves comparing PCM-DE with other algorithms.

Data availability

The data presented in this study are available through email upon request to the corresponding author.

Received: 3 January 2025; Accepted: 3 March 2025
Published online: 13 March 2025

References

1. Sun, S., Su, Y., Yin, C. & Jermsittiparsert, K. Optimal parameters estimation of PEMFCs model using converged moth search algorithm. *Energy Rep.* **6**, 267–275. https://doi.org/10.1016/j.egyr.2020.06.002 (2020).
2. Hao, P. & Sobhani, B. Application of the improved chaotic grey wolf optimization algorithm as a novel and efficient method for parameter estimation of solid oxide fuel cells model. *Int. J. Hydrogen Energy* **46**(73), 36674–36687. https://doi.org/10.1016/j.ijhydene.2021.08.174 (2021).
3. Yu, Y., Chen, H. & Zhang, T. A gas starvation diagnosis method of PEM fuel cells based on adaptive network-based fuzzy inference system (ANFIS). *Energy Proc.* **22**, 9413–9419. https://doi.org/10.46855/energy-proceedings-9413 (2021).
4. Du, Y., Yang, J., Xu, J., Yuan, J., Feng, K. & Zhang, S. Fault diagnosis based on the adaptive network fuzzy inference system for power system of offshore platform. In *Proceedings of the 34th Chinese control and decision conference (CCDC 2022)*. https://doi.org/10.1109/CCDC55256.2022.10033515 (2022).
5. Xing, Y., Na, J., Chen, M., Costa-Castello, R. & Roda, V. Adaptive nonlinear parameter estimation for a proton exchange membrane fuel cell. *IEEE Trans. Power Electron.* **37**(8), 9284–9295. https://doi.org/10.1109/TPEL.2022.3155573 (2022).
6. Yang, F., Li, Y., Chen, D., Hu, S. & Xu, X. Parameter identification of PEMFC steady-state model based on p-dimensional extremum seeking via simplex tuning optimization method. *Energy* **292**, 130601. https://doi.org/10.1016/j.energy.2024.130601 (2024).
7. Fathy, A., Babu, T. S., Abdelkareem, M. A., Rezk, H. & Yousri, D. Recent approach based heterogeneous comprehensive learning Archimedes optimization algorithm for identifying the optimal parameters of different fuel cells. *Energy* **248**, 123587. https://doi.org/10.1016/j.energy.2022.123587 (2022).
8. Mitra, U., Arya, A. & Gupta, S. A comprehensive and comparative review on parameter estimation methods for modelling proton exchange membrane fuel cell. *Fuel* **335**, 127080. https://doi.org/10.1016/j.fuel.2022.127080 (2023).
9. Guo, M. et al. Online split-phase identification of asymmetric parameters between distribution lines and ground for unbalanced voltage compensation based on power electronics. *IEEE Trans. Power Electron.* **39**(8), 6799–6812. https://doi.org/10.1109/TPEL.2024.3396216 (2024).
10. Yuan, Y. et al. Attack-defense strategy assisted osprey optimization algorithm for PEMFC parameters identification. *Renew. Energy* **225**, 120211. https://doi.org/10.1016/j.renene.2024.120211 (2024).
11. Singla, M. K., Nijhawan, P. & Oberoi, A. S. Parameter estimation of proton exchange membrane fuel cell using a novel meta-heuristic algorithm. *Environ. Sci. Pollut. Res.* **28**(26), 35225–35239. https://doi.org/10.1007/s11356-021-13097-0 (2021).
12. Ghosh, S., Routh, A., Hembrem, P., Rahaman, M. & Ghosh, A. Dynamic ant colony optimization algorithm for parameter estimation of PEM fuel cell. *Eng. Res. Express* **6**(2), 026001. https://doi.org/10.1088/2631-8695/ad53a3 (2024).
13. Singh, B., Nijhawan, P., Singla, M. K., Gupta, J. & Singh, P. Hybrid algorithm for parameter estimation of fuel cell. *Int. J. Energy Res.* **46**(8), 10348–10367. https://doi.org/10.1002/er.7863 (2022).
14. Singla, M. K. et al. Parameter estimation of fuel cells using a hybrid optimization algorithm. *Sustainability* **15**(8), 6676. https://doi.org/10.3390/su15086676 (2023).
15. Singla, M. K. et al. An enhanced efficient optimization algorithm (EINFO) for accurate extraction of proton exchange membrane fuel cell parameters. *Soft Comput.* **27**(14), 4201–4220. https://doi.org/10.1007/s00500-023-08092-1 (2023).
16. Chen, Y., Pi, D., Wang, B., Chen, J. & Xu, Y. Bi-subgroup optimization algorithm for parameter estimation of a PEMFC model. *Expert Syst. Appl.* **196**, 116646. https://doi.org/10.1016/j.eswa.2022.116646 (2022).
17. Sultan, H. M., Menesy, A. S., Hassan, M., Jurado, F. & Kamel, S. Standard and Quasi Oppositional bonobo optimizers for parameter extraction of PEM fuel cell stacks. *Fuel* **340**, 127586. https://doi.org/10.1016/j.fuel.2023.127586 (2023).
18. Krishnan, P. & Aravindhar, J. Self-adaptive PSO memetic algorithm for multi objective workflow scheduling in hybrid cloud. *Int. Arab J. Inf. Technol. (IAJIT)* **16**(05), 138–145 (2019).
19. Xiong, G., Zhang, J., Shi, D. & Yuan, X. A simplified competitive swarm optimizer for parameter identification of solid oxide fuel cells. *Energy Convers. Manag.* **203**, 112204. https://doi.org/10.1016/j.enconman.2019.112204 (2020).
20. Yang, L. et al. A review on thermal management in proton exchange membrane fuel cells: Temperature distribution and control. *Renew. Sustain. Energy Rev.* **187**, 113737. https://doi.org/10.1016/j.rser.2023.113737 (2023).
21. Abdelmalek, S., Dali, A., Bettayeb, M. & Bakdi, A. A new effective robust nonlinear controller based on PSO for interleaved DC–DC boost converters for fuel cell voltage regulation. *Soft Comput.* **24**(22), 17191–17205. https://doi.org/10.1007/s00500-020-04996-4 (2020).
22. Sun, Z. et al. Proton exchange membrane fuel cell model parameter identification based on dynamic differential evolution with collective guidance factor algorithm. *Energy* **216**, 119056. https://doi.org/10.1016/j.energy.2020.119056 (2021).
23. Li, Y., Yang, F., Chen, D., Hu, S. & Xu, X. Thermal-physical modeling and parameter identification method for dynamic model with unmeasurable state in 10-kW scale proton exchange membrane fuel cell system. *Energy Convers. Manag.* **276**, 116580. https://doi.org/10.1016/j.enconman.2022.116580 (2023).
24. Rehman, A. U., Ryu, S.-W., Park, H. & Jung, J.-W. A critical review of recent industrial developments, trends, and future perspectives of power electronic systems: Fuel cell electric vehicles. *IEEE Trans. Ind. Inf.* **20**(4), 3020–3032. https://doi.org/10.1109/TII.2023.3347736 (2024).
25. Bankupalli, P. T., Ghosh, S., Sahu, L. K. & Dwivedi, A. K. Piecewise temperature-dependent electrical equivalent modeling of PEM fuel cell for power conditioning unit design using fuzzy clustering and hybrid optimization. *Energy Sources Part A Recovery Util. Environ. Effects* https://doi.org/10.1080/15567036.2021.1903619 (2021).
26. Li, Q., Yang, W., Yin, L. & Chen, W. Real-time implementation of maximum net power strategy based on sliding mode variable structure control for proton-exchange membrane fuel cell system. *IEEE Trans. Transp. Electrif.* **6**(1), 113–121. https://doi.org/10.1109/TTE.2020.2970835 (2020).
27. Kashefi, H., Sadegheih, A., Mostafaeipour, A. & Mohammadpour Omran, M. Parameter identification of solar cells and fuel cells using improved social spider algorithm. *COMPEL Int. J. Comput. Math. Electr. Electron. Eng.* **40**(2), 563–579. https://doi.org/10.1108/COMPEL-12-2019-0495 (2020).
28. Lekouaghet, B., Khelifa, M. A. & Boukabou, A. Precise parameter estimation of PEM fuel cell via weighted mean of vectors optimizer. *J. Comput. Electron.* **23**(5), 1663–1680. https://doi.org/10.1007/s10825-024-02204-2 (2024).
29. Tummala, A. S. L. V., Polumahanthi, N., Khan, B. & Ali, A. Accurate parameters identification of proton exchange membrane fuel cell using Young's double-slit experiment optimizer. *Front. Energy Res.* **12**, 1384649. https://doi.org/10.3389/fenrg.2024.1384649 (2024).
30. Ebrahimi, S. M., Hasanzadeh, S. & Khatibi, S. Parameter identification of fuel cell using repairable grey wolf optimization algorithm. *Appl. Soft Comput.* **147**, 110791. https://doi.org/10.1016/j.asoc.2023.110791 (2023).
31. Fathy, A., Abdel Aleem, S. H. E. & Rezk, H. A novel approach for PEM fuel cell parameter estimation using LSHADE-EpSin optimization algorithm. *Int. J. Energy Res.* **45**(5), 7035–7052. https://doi.org/10.1002/er.6282 (2021).

32. Alizadeh, M. & Torabi, F. Precise PEM fuel cell parameter extraction based on a self-consistent model and SCCSA optimization algorithm. *Energy Convers. Manag.* **229**, 113777. https://doi.org/10.1016/j.enconman.2020.113777 (2021).
33. Chen, J.-H. et al. Modeling and temperature control of a water-cooled PEMFC system using intelligent algorithms. *Appl. Energy* **372**, 123790. https://doi.org/10.1016/j.apenergy.2024.123790 (2024).
34. Bai, Q. & Li, H. The application of hybrid cuckoo search-grey wolf optimization algorithm in optimal parameters identification of solid oxide fuel cell. *Int. J. Hydrogen Energy* **47**(9), 5962–5975. https://doi.org/10.1016/j.ijhydene.2021.11.216 (2022).
35. Wu, K., Zhu, J., & Jiang, B. Hybrid fuzzy controller design on oxygen excess ratio control of PEMFC air feed system by using PSO algorithm. In *Proceedings of the 33rd Chinese control and decision conference (CCDC 2021)*. https://doi.org/10.1109/CCDC52312.2021.9601625 (2021).
36. Miao, D., Chen, W., Zhao, W. & Demsas, T. Parameter estimation of PEM fuel cells employing the hybrid grey wolf optimization method. *Energy* **193**, 116616. https://doi.org/10.1016/j.energy.2019.116616 (2020).
37. Lin, M., Yang, C. & Li, D. Hybrid strategy-based model parameter estimation of irregular-shaped underwater vehicles for predicting velocity. *Robot. Auton. Syst.* **127**, 103480. https://doi.org/10.1016/j.robot.2020.103480 (2020).
38. Zhang, B. et al. Parameter identification of proton exchange membrane fuel cell based on swarm intelligence algorithm. *Energy* **283**, 128935. https://doi.org/10.1016/j.energy.2023.128935 (2023).
39. Ji, K. et al. Uniform initialization in response space for PSO and its applications. *Appl. Math. Comput.* **431**, 127351. https://doi.org/10.1016/j.amc.2022.127351 (2022).
40. Yang, F. et al. A review on mass transfer in multiscale porous media in proton exchange membrane fuel cells: Mechanism, modeling, and parameter identification. *Energies* **16**(8), 3547. https://doi.org/10.3390/en16083547 (2023).
41. Yang, B. et al. A critical survey on proton exchange membrane fuel cell parameter estimation using meta-heuristic algorithms. *J. Clean. Prod.* **265**, 121660. https://doi.org/10.1016/j.jclepro.2020.121660 (2020).
42. Sultan, H. M., Menesy, A. S., Alqahtani, M., Khalid, M. & Zaki Diab, A. A. Accurate parameter identification of proton exchange membrane fuel cell models using different metaheuristic optimization algorithms. *Energy Rep.* **10**, 145–160. https://doi.org/10.1016/j.egyr.2023.11.007 (2023).
43. Sultan, H. M., Menesy, A. S., Korashy, A., Hussien, A. G. & Kamel, S. Enhancing parameter identification for proton exchange membrane fuel cell using modified manta ray foraging optimization. *Energy Rep.* **12**, 251–266. https://doi.org/10.1016/j.egyr.2024.07.063 (2024).
44. Yuan, H., Dai, H., & Wei, X. Parameter identification for a proton exchange membrane fuel cell model. *SAE Technical Papers*, 0858. https://doi.org/10.4271/2020-01-0858 (2020).
45. Wei, T., Chang, G., Dai, H., Yuan, H., Zhao, L., Wei, X., & Zhou, J. Understanding the transient behavior and consistency evolution of PEMFC from the perspective of temperature. *SAE Technical Papers*, 0189. https://doi.org/10.4271/2022-01-0189 (2022).
46. Song, Z., Ren, C. & Meng, Z. Differential evolution with perturbation mechanism and covariance matrix-based stagnation indicator for numerical optimization. *Swarm Evolut. Comput.* **84**, 101447. https://doi.org/10.1016/j.swevo.2023.101447 (2024).
47. Menesy, A. S., Sultan, H. M., Selim, A., Ashmawy, M. G. & Kamel, S. Developing and applying chaotic Harris Hawks optimization technique for extracting parameters of several proton exchange membrane fuel cell stacks. *IEEE Access* **8**, 1146–1159. https://doi.org/10.1109/ACCESS.2019.2961811 (2020).
48. Yongguang, C. & Guanglei, Z. New parameters identification of proton exchange membrane fuel cell stacks based on an improved version of African vulture optimization algorithm. *Energy Rep.* **8**(75), 3030–3040. https://doi.org/10.1016/j.egyr.2022.02.066 (2022).
49. Hasanien, H. M. et al. Precise modeling of PEM fuel cell using a novel Enhanced Transient Search Optimization algorithm. *Energy* **247**, 123530 (2022).
50. Meng, Z. & Yang, C. Two-stage differential evolution with novel parameter control. *Inform. Sci.* **596**, 321–342. https://doi.org/10.1016/j.ins.2022.03.043 (2022).
51. Meng, Z., Zhong, Y., Mao, G. & Liang, Y. PSO-sono: A novel PSO variant for single-objective numerical optimization. *Inform. Sci.* **586**, 176–191. https://doi.org/10.1016/j.ins.2021.11.076 (2022).
52. Meng, Z., Zhong, Y. & Yang, C. Cs-de: Cooperative strategy based differential evolution with population diversity enhancement. *Inform. Sci.* **577**, 663–696. https://doi.org/10.1016/j.ins.2021.07.080 (2021).
53. Brest, J., Maučec, M. S. & Bošković, B. Single objective real parameter optimization: Algorithm jSO. In *2017 IEEE congress on evolutionary computation (CEC)*, IEEE, pp. 1311–1318. https://doi.org/10.1109/CEC.2017.7969456 (2017).
54. Abdel-Basset, M. et al. Exponential distribution optimizer (EDO): A novel math-inspired algorithm for global optimization and engineering problems. *Artif. Intell. Rev.* **56**, 9329–9400. https://doi.org/10.1007/s10462-023-10403-9 (2023).
55. Tanabe, R. & Fukunaga, A. S. Improving the search performance of SHADE using linear population size reduction. In *2014 IEEE congress on evolutionary computation (CEC)*, IEEE, pp. 1658–1665. https://doi.org/10.1109/CEC.2014.6900380 (2014).
56. Zhang, G. & Shi, Y. Hybrid sampling evolution strategy for solving single objective bound constrained problems. In *2018 IEEE congress on evolutionary computation (CEC)*, IEEE, pp. 1–7. https://doi.org/10.1109/CEC.2018.8477908 (2018).
57. Meng, Z., Chen, Y., Li, X., Yang, C. & Zhong, Y. Enhancing quasi-affine transformation evolution (QUATRE) with adaptation scheme on numerical optimization. *Knowl.- Based Syst.* **197**, 105908. https://doi.org/10.1016/j.knosys.2020.105908 (2020).
58. Bujok, P. & Kolenovsky, P. Eigen crossover in cooperative model of evolu tionary algorithms applied to CEC 2022 single objective numerical optimization. In *2022 IEEE congress on evolutionary computation (CEC)*, IEEE, pp. 1–8. https://doi.org/10.1109/CEC55065.2022.9870433 (2022).
59. Rowe, A. & Li, X. Mathematical modeling of proton exchange membrane fuel cells. *J. Power Sources* **102**(1–2), 82–96. https://doi.org/10.1016/S0378-7753(01)00798-4 (2001).
60. Correa, J. M., Farret, F. A., Canha, L. N. & Simoes, M. G. An electrochemical-based fuel-cell model suitable for electrical engineering automation approach. *IEEE Trans. Ind. Electron.* **51**(5), 1103–1112. https://doi.org/10.1109/TIE.2004.834972 (2004).
61. Aouali, F. Z. et al. Analytical modelling and experimental validation of proton exchange membrane electrolyser for hydrogen production. *Int. J. Hydrog. Energy* **42**(2), 1366–1374. https://doi.org/10.1016/j.ijhydene.2016.03.101 (2017).
62. Amphlett, J. C. et al. Performance modeling of the Ballard Mark IV solid polymer electrolyte fuel cell: I. Mechanistic model development. *J. Electrochem. Soc.* **142**(1), 1–8. https://doi.org/10.1149/1.2043866 (1995).
63. Mann, R. F. et al. Development and application of a generalised steady state electrochemical model for a PEM fuel cell. *J. Power Sources* **86**(1–2), 173–180. https://doi.org/10.1016/S0378-7753(99)00484-X (2000).
64. Amphlett, J. C. et al. Performance modeling of the Ballard Mark IV solid polymer electrolyte fuel cell: II. Empirical model development. *J. Electrochem. Soc.* **142**(1), 9–15. https://doi.org/10.1149/1.2043959 (1995).
65. Mo, Z.-J., Zhu, X.-J., Wei, L.-Y. & Cao, G.-Y. Parameter optimization for a PEMFC model with a hybrid genetic algorithm. *Int. J. Energy Res.* **30**, 585–597. https://doi.org/10.1002/er.1170 (2006).
66. Alatas, B. Chaotic harmony search algorithms. *Appl. Math. Comput.* **216**(3), 2687–2699. https://doi.org/10.1016/j.amc.2010.03.114 (2010).
67. Nguyen, T. V. & White, R. E. A water and heat management model for proton-exchange-membrane fuel cells. *J. Electrochem. Soc.* **140**(8), 2178–2186. https://doi.org/10.1149/1.2220792 (1993).
68. El-Fergany, A. A. Electrical characterisation of proton exchange membrane fuel cells stack using grasshopper optimiser. *IET Renew. Power Gener.* **12**(1), 9–17. https://doi.org/10.1049/iet-rpg.2017.0232 (2017).
69. Ali, M., El-Hameed, M. A. & Farahat, M. A. Effective parameters identification for polymer electrolyte membrane fuel cell models using grey wolf optimizer. *Renew. Energy* **111**, 455–462. https://doi.org/10.1016/j.renene.2017.04.036 (2017).

70. Zhang, J. & Sanderson, A. C. JADE: Adaptive differential evolution with optional external archive. *IEEE Trans. Evol. Comput.* **13**(5), 945–958. https://doi.org/10.1109/TEVC.2009.2014613 (2009).
71. Tanabe, R. & Fukunaga, A. Success-history based parameter adaptation for differential evolution, In *2013 IEEE congress on evolutionary computation*, IEEE, pp. 71–78. https://doi.org/10.1109/CEC.2013.6557555 (2013).

Acknowledgements
This research is scientifically supported by the Deanship of Scientific Research at Zarqa University, Jordan.

Author contributions
M.A., P.J., A., S.P.A., and S.B.P. conceptualized and designed the study. M.A., P.J., and A. developed the PCM-DE algorithm and implemented the computational framework. G.G. and A.F.A. conducted the validation experiments and analyzed the data. M.K. and S.B.P. prepared the PEMFC parameter estimation models and contributed to statistical analyses. A.P. and M.K. prepared Figs. 1, 2, 3, 4, 5 and 6 and contributed to drafting sections of the manuscript. M.A., P.J., and A. wrote the main manuscript text. All authors reviewed the manuscript, provided critical revisions, and approved the final version.

Funding
The Researchers would like to thank the Deanship of Graduate Studies and Scientific Research at Qassim University for financial support (QU-APC-2025).

Declarations

Competing interests
The authors declare no competing interests.

Additional information
Correspondence and requests for materials should be addressed to M.A., G.G., A.F.A. or M.K.

Reprints and permissions information is available at www.nature.com/reprints.

Publisher's note Springer Nature remains neutral with regard to jurisdictional claims in published maps and institutional affiliations.